Rectified Barotropic Flow over a Submarine Canyon

NICOLAS PERÉNNE, JACQUES VERRON, AND DOMINIQUE RENOUARD

Laboratoire des Ecoulements Geophysiques et Industriels, CNRS, Institut de Mecanique de Grenoble, Grenoble, France

DON L. BOYER AND XIUZHANG ZHANG

Environmental Fluid Dynamics Program and Department of Mechanical and Aerospace Engineering, Arizona State University, Tempe, Arizona

(Manuscript received 29 November 1995, in final form 3 February 1997)

ABSTRACT

The effect of an isolated canyon interrupting a long continental shelf of constant cross section on the along-isobath, oscillatory motion of a homogeneous, incompressible fluid is considered by employing laboratory experiments (physical models) and a numerical model. The laboratory experiments are conducted in two separate cylindrical test cells of 13.0- and 1.8-m diameters, respectively. In both experiments the shelf topography is constructed around the periphery of the test cells, and the oscillatory motion is realized by modulating the rotation rate of the turntables. The numerical model employs a long shelf in a rectangular Cartesian geometry. It is found from the physical experiments that the oscillatory flow drives two characteristic flow patterns depending on the values of the temporal Rossby number, Ro_t, and the Rossby number, Ro. For sufficiently small Ro_t, and for the range of Ro investigated, cyclonic vortices are formed during the right to left portion of the oscillatory cycle, facing toward the deep water, on (i) the inside right and (ii) the outside left of the canyon; that is, the cyclone regime. For sufficiently large Ro_t and the range of Ro studied, no closed cyclonic eddy structures are formed, a flow type designated as cyclone free.

The asymmetric nature of the right to left and left to right phases of the oscillatory, background flow leads to the generation of a mean flow along the canyon walls, which exits the canyon region on the right, facing toward the deep water, and then continues along the shelf break before decaying downstream. A parametric study of the physical and numerical model experiments is conducted by plotting the normalized maximum mean velocity observed one canyon width downstream of the canyon axis against the normalized excursion amplitude X. These data show good agreement between the physical experiments and the numerical model. For $X \geq 0.4$, the normalized, maximum, mean velocity is independent of X and is roughly equal to 0.6; i.e., the maximum mean velocity is approximately equal to the mean forcing velocity over one half of the oscillatory cycle (these experiments are all of the cyclone flow type). For $X \leq 0.4$, the normalized maximum mean velocity separates into (i) a lower branch for which the mean flow is relatively small and increases with X (cyclone-free flow type) and (ii) an upper branch for which the mean flow is relatively large and decreases with X (cyclone flow type).

The time-dependent nature of the large-scale eddy field for a numerical model run in the cyclone regime is shown to agree well qualitatively with physical experiments in the same regime. Time-mean velocity and streamfunction fields obtained from the numerical model are also shown to agree well with the laboratory experiments. Comparisons are also made between the present model findings and some oceanic observations and findings from other models.

1. Introduction

The recent past has seen a surge of interest by the oceanographic community to better understand the physical and biological processes (and their interaction) at work in the coastal environment. This derives from the obvious fact that coastal waters are intensely used for commercial fishing, transportation, mineral extraction, and recreation. A particularly interesting and complex question in near coastal oceanography is the nature of the current systems within submarine canyons and the effect such canyons have on the characteristics of currents in their vicinity. The present study is a combined laboratory–numerical model investigation of an idealized system aimed at providing insight into some of the various physical phenomena that may come into play in the vicinity of submarine canyons. The geometry considered is that of a long continuous shelf–shelf break–continental slope of constant cross section, interrupted by a smooth canyon. The fluid is taken as homogeneous and incompressible and the system is forced by a barotropic, alongshelf, oscillatory background flow.

Corresponding author address: Dr. Don L. Boyer, Dept. of Mechanical and Aerospace Engineering, College of Engineering and Applied Science, Arizona State University, Box 876106, Tempe, AZ 85287-6106.
E-mail: don.boyer@asu.edu

Because of the difficulties of making measurements in submarine canyons, especially on their steep slopes, it is not surprising that early measurements concentrated mainly on locations along the canyon axes. The earliest current measurements were taken in a number of Georges Bank canyons by Stetson (1936) and in canyons off the California coast by Shepard et al. (1939). The underlying physics governing the currents observed was not readily apparent from the observational data; for example, what determines up- or downcanyon mean flow? Freeland and Denman (1982) gave observational evidence that a canyon can play an important role in determining the nature of the motion system away from the canyon itself; see also Freeland and McIntosh (1989). A synoptic five-day hydrographic study of the region in the vicinity of Wilmington Canyon was made by Church et al. (1984).

Hickey et al. (1986) discussed measurements from a field study in Quinault Canyon off the coast of Washington directed to examining processes controlling subtidal fluctuations in suspended particulate concentrations. They found correlations between variations in the flow in the canyon and the vertical excursions of turbidity with the alongshore circulation patterns. Hickey (1989), also reporting on measurements in Quinault, found that upcanyon flows were observed in the upper canyon and downcanyon flows in the lower canyon. Kinsella et al. (1987) presented observations of the interaction of the Labrador Current with Carson Canyon located along the edge of the Grand Bank of Newfoundland. The time-averaged current measurements showed that the flow–topography interaction over the canyon is nonlinear and that the mean current crosses isobaths; that is, the Rossby number is of order unity in the vicinity of the canyon.

Observations of mean and tidal currents within Baltimore Canyon and its vicinity were reported by Hunkins (1988). The background flow (10–15 cm s^{-1}) was toward the southwest along the shelf break, with tidal current velocities in the direction (onshore) of the major axis of the M_2 ellipse being 9 cm s^{-1}. It was found that the mean currents above the canyon in the upper 100 m were little affected by the presence of the canyon. At 50 m above the bottom along the northeast side of the canyon there appeared to be an anticlockwise circulation along the depth contours of the canyon (see his Fig. 8). Along the canyon axis near the floor there was a convergent circulation with downcanyon flow near the head and upcanyon motion near the mouth (see his schematic diagram of Fig. 10). Tides dominated the flow within the canyon and its vicinity. The tides were primarily semidiurnal and had their largest amplitudes along the canyon axis near the floor. The tides near the shelf break were found to have slightly less amplitude, while those on the adjacent slopes were much weaker. While the tides were found to be rotary on the shelf, they were rectilinear and aligned with the canyon axis in the interior. The strongest mean currents were found along the canyon axis near the floor; their origins were not understood but the author speculated that the upcanyon flow near the mouth may have been due to tidal rectification. The present experiments provide some evidence in support of this conjecture.

Noble and Butman (1989) reported on measurements of subtidal currents within and in the vicinity of Lydonia Canyon located to the south of Georges Bank. They found that the subtidal currents (periods between 2.5 and 32 days) over the shelf and slope ranged from 10 to 30 cm s^{-1} and within the canyon were of the order of 5 cm s^{-1}. They concluded that currents within the canyon were driven by the cross-shelf pressure gradient associated with the geostrophic alongshelf flow. The alongshelf currents were driven by the large-scale component of the wind field and showed an oscillatory nature.

Durrieu de Madron (1994) studied the flow in Grand-Rhone Canyon along the Mediterranean coast. The background current was along the slope but did not extend up on the shelf and the canyon was on the right of this current. The background current was observed to turn cyclonically into the canyon on the upstream side and an anticyclonic current was observed near the head of the canyon. Downcanyon flow was observed along the floor near the canyon mouth. The influence of tides was found to be very small in this region.

Hickey (1997) has reported on detailed measurements taken in Astoria Canyon located along the Washington coast. She found that upwelling in the canyon is highly correlated and in phase with the alongshelf, wind-driven current to the south. When upwelling is initiated, she found a local increase in the cyclonic vorticity on the upstream side of the canyon near its rim. She further observed that during upwelling the flow (i) at depths above ~100 m above the canyon rim was undisturbed by the canyon, (ii) at depths of 40–100 m above the canyon exhibits a cyclonic circulation pattern, and (iii) within the canyon was anticlockwise along the canyon walls.

Thus, while numerous field observations of canyon flows have been made, they are insufficient to obtain a coherent picture of individual physical processes. Referring to the field measurements made to date, Hickey (1995) states, ''The observations have been made over different time periods and in different seasons, at different heights above the bottom and in different parts of the canyons (and in different canyons). Not surprisingly, therefore no firm understanding of driving mechanisms for mean flow near the canyon floor has emerged. It is safe to say that at this point in time, the direction of the mean flow above the floor of a specific canyon cannot be predicted with any reasonable certainty.''

Some analytical, numerical, and laboratory investigations of canyon circulations have been made. Klinck (1988) developed an analytical model of the interaction of a homogeneous geostrophic current with a transverse submarine canyon. The canyon was a channel of rect-

angular cross section on the bottom of a flat ocean. The flow was driven by an alongcanyon pressure gradient as introduced by a sloping free surface. The solutions for a canyon of arbitrary width are composed of standing waves over the canyon and radiating waves on the canyon sides. Klinck (1989) studied the geostrophic adjustment to a stratified current crossing a canyon. He showed that the width of the canyon determines the strength of the cross-canyon flow and in turn the effect of the canyon on the coastal current. The interaction is shown to be smaller for canyon widths smaller than the current width or the internal radius of deformation.

In a recent paper, Klinck (1996), using the Haidvogel et al. (1991) semispectral primitive equation model (SPEM), conducted a numerical investigation of stratified flow in and near canyons driven by alongshore currents normal to the canyon axes. He considered four cases, two for the driving current having the canyon on the right, facing downstream, and two with the canyon on the left. For each direction, cases of weak and strong stratification were considered. Changes in the strength of the stratification had only modest effects on the overall flow patterns. Changes in the flow direction with respect to the canyon orientation, however, had significant qualitative and quantitative effects. For the case of the canyon on the right, the flow had a rather smooth pattern with the tendency of streamlines to more or less ''follow the topography.'' For the case of the canyon on the left, the deep flow showed a tendency to advect into the canyon, while the upper-level flow entered the canyon in a rather regular way with the current being distributed along the shelf. When leaving the canyon, however, the flow split into a strong jet on the shelf and another strong current along the shelf contours but quite far offshore. These model results demonstrate the significant effect flow direction can have on a flow interacting with a coastal canyon.

In a recent study, Allen (1996) reported on a linear theory of wind-driven flow past a canyon of infinitesimal width but finite length. She also presented numerical results for counterpart canyons of narrow but finite width and finite length. The results show that the linear theory is a reasonable approximation to the numerical experiments for a canyon that is narrow compared to the baroclinic Rossby radius.

Haidvogel and Beckman (1995) have considered numerically the problem of residual (time mean) currents driven by oscillatory alongshelf winds over a continental shelf/slope in the presence of an across-shelf canyon (a model similar to, but not exactly the same as, the barotropic oscillatory forcing considered herein). They compared five different numerical models, including the Geophysical Fluid Dynamics Laboratory Modular Ocean Model (GFDLM: Bryan 1969; Cox 1984), the Miami Isopycnic Coordinate Ocean Model (MICOM: Bleck et al. 1992), the Princeton Ocean Model (POM: Blumberg and Mellor 1987), the Spectral Element Model (SEM: Iskandarani et al. 1995), and the Semispectral Primitive Equation Model (SPEM: Haidvogel et al. 1991; Hedstrom 1994). Without going into a great deal of detail, it is fair to say that, for the homogeneous case, the results for the residual flows agreed quite well qualitatively, but not quantitatively. As might be expected, the introduction of stratification only served to increase model–model differences leading to flow patterns that differed substantially, both qualitatively and quantitatively, for the various models.

Models and laboratory experiments have demonstrated that internal waves are amplified within submarine canyons; for example, Hotchkiss and Wunsch (1982), Baines (1983), and Grimshaw et al. (1985). This amplification has been observed in the Hudson (Hotchkiss and Wunsch 1982) and Quinault (Hickey 1989) Canyons. Submarine canyons may also be sources of strong boundary turbulence. Lueck and Osborn (1985), for example, measured bottom boundary layers as thick as 170 m in Monterey Canyon. Numerous theoretical studies have also addressed the matter of submarine canyons being the source or a factor in modifying the structure of coastal trapped waves; for example, Allen (1976), Wang (1980), and Wilken and Chapman (1990).

Laboratory work on flows in and near submarine canyons has been minimal. One significant study is that of Baines (1983) who conducted experiments (nonrotating) on the generation of internal waves by tides in a stratified fluid in a narrow canyon (i.e., the width of the canyon is much smaller than the wavelength). He showed that the observed wave motion in the canyon was forced by the incident barotropic tide from the deep ocean as well as the internal wave reflected back into the canyon from its open mouth. Reviews of various studies concerning physical processes at work in coastal canyons have been made by Inman et al. (1976), Cannon and Lagerloef (1983), Hickey (1995), and Huthnance (1995).

In summary, there are a myriad of physical processes at work in submarine canyons and the associated physical phenomena are not well understood. In particular, not a great deal of synoptic, time-dependent data concerned with the nature of currents within and near submarine canyons is available. Clearly, the driving of these currents comes from a variety of sources having a broad range of time and length scales, including (i) currents associated with the ocean's general circulation including advecting mesoscale structures, (ii) wind-driven currents, (iii) thermohaline effects, (iv) gravity waves, and (v) tides; see Huthnance (1995). Furthermore, such currents are influenced by the background stratification of the ocean, the earth's rotation, and the complex bathymetry (steep and tall) of the canyon itself. In the spirit of better understanding the effects of some particular physical processes, we consider isolating some of them and totally neglecting others. In particular, we consider herein barotropic, alongshelf, oscillatory forcing past the canyon and inquire as to the nature of the resulting flow fields. In doing so we totally neglect such

effects as stratification and wind-driven currents and other background flows. While the oscillatory character of the background flow is motivated by tidal effects, it is noted that the present study mainly addresses subtidal frequencies. For very slow oscillations, the current can be considered a slowly accelerating–decelerating one with the canyon on the right for half the cycle and on the left for the other half, that is, in some sense similar to the Klinck (1996) numerical model but without the effects of stratification.

As one will note, the present physical system leads to current fields that are associated with significant mean (rectified) flows. It thus is in order to provide a brief overview of the literature on this topic. Tidal rectification has been observed at numerous places in the world's oceans. Butman et al. (1982) and Tee (1985) reported on an anticyclonic mean circulation around Georges Bank off the northeast coast of the United States, with this mean flow being along isobaths and being depth and seasonally dependent. Garreau and Mazé (1992) discussed similar tide-generated mean flow observations near La Chapelle Bank off the northwest coast of France. Tide-induced rectified flows have also been observed around Bermuda (Stommel 1954), Fieberling Guyot in the North Pacific (Genin et al. 1989; Ericksen 1991), in the Bay of Biscay (Pingree and Le Cann 1990), and in the Straits of Dover (Brylinski and Lagadeuc 1990).

There is a growing and substantial literature of theoretical and numerical model studies addressed to (i) determining the physical mechanisms leading to the generation of mean flows by tidal motions and (ii) obtaining estimates of the mean flow generated in terms of the forcing properties of the tides, the ocean floor bathymetry, the Coriolis parameter, and the nature of the viscous effects that are essential for rectification to occur. One physical system studied extensively is that of the incidence of tidal oscillations onto an infinitely long ridge. Depth-independent models for this geometry include those of Huthnance (1973, 1981), Zimmerman (1978, 1980), Tee (1979, 1980), Loder (1980), and Loder and Wright (1985). It is generally accepted that friction is required to generate mean flows and that the nature of the mean flows generated depends on the particular frictional parameterization used, but not on the magnitude of the friction itself.

Motivated by oceanic observations of mean flows generated near Fieberling Guyot, Boyer et al. (1991) conducted a laboratory study of rectified flows induced by a homogeneous, rotating, oscillating barotropic fluid past an obstacle of revolution. This was extended to include the effects of background stratification by Boyer and Zhang (1990) and Zhang and Boyer (1993). Recently Verron et al. (1995) conducted laboratory and accompanying numerical model experiments of alongshore, oscillatory currents of a homogeneous rotating fluid past an elongated topographic feature located adjacent to a vertical coastline.

Haidvogel and Brink (1986) conducted a series of numerical experiments on a periodic, wind-driven, depth-averaged barotropic flow along a long continental shelf topography having periodic bottom relief in both the along- and cross-isobath directions. They argue that for southward flow along the west coast of the United States, for example, shelf lee waves will form and propagate energy to infinity creating a topographic drag on the background flow (e.g., Brink 1986). On the other hand, northward flow will not result in such lee waves and hence no topographic drag, based on this phenomenon, will be in evidence. This asymmetry in the topographic drag leads to a mean flow in the northward direction for periodic north to south forcing. Such an asymmetry in topographic drag leading to a residual flow is in evidence in the present experiments.

The scientific questions to be addressed in the present study are, by establishing along-isobath motions past a canyon on an otherwise continuous shelf break geometry, (i) what are the principal effects on the time-dependent motion fields in the vicinity of the canyon; (ii) what is the nature of any mean motion field that might be so-generated; and (iii) to what degree are some of the present observations seen in nature and other modeling studies? The plan for the presentation is to first discuss the physical model, the experimental techniques employed, and the governing dimensionless parameters in section 2. The physical model results will then be presented in section 3. The numerical model will be discussed in section 4, and the numerical model findings will be given in section 5. A brief discussion of the relation between the present study and oceanographic observations and other models is given in section 6, with a summary and concluding remarks made in section 7.

2. Physical model and experimental techniques

This communication addresses, by laboratory experiments and a numerical model, the question of the motion fields resulting from the interaction of oscillatory currents along a continental shelf break interrupted by a single isolated canyon (i.e., a depression in the alongshelf direction). The problem of avoiding significant end effects in the physical models is minimized by considering a continuous annular topography of constant cross section, interrupted by a canyon, placed along the periphery of a cylindrical test cell; see Fig. 1a. While, as discussed below, for certain governing parameter conditions, the rectified flow (clockwise for anticlockwise rotation) generated in the vicinity of the canyon can propagate around the entire test cell and thus influence the ''upstream boundary condition,'' this effect is weak and is not considered of substantial importance in determining the phenomena investigated. The numerical model uses a rectangular channel configuration of sufficient length to conclude that end effects are not unduly influencing the motion field; see Fig. 1b.

Experiments were conducted in two separate facili-

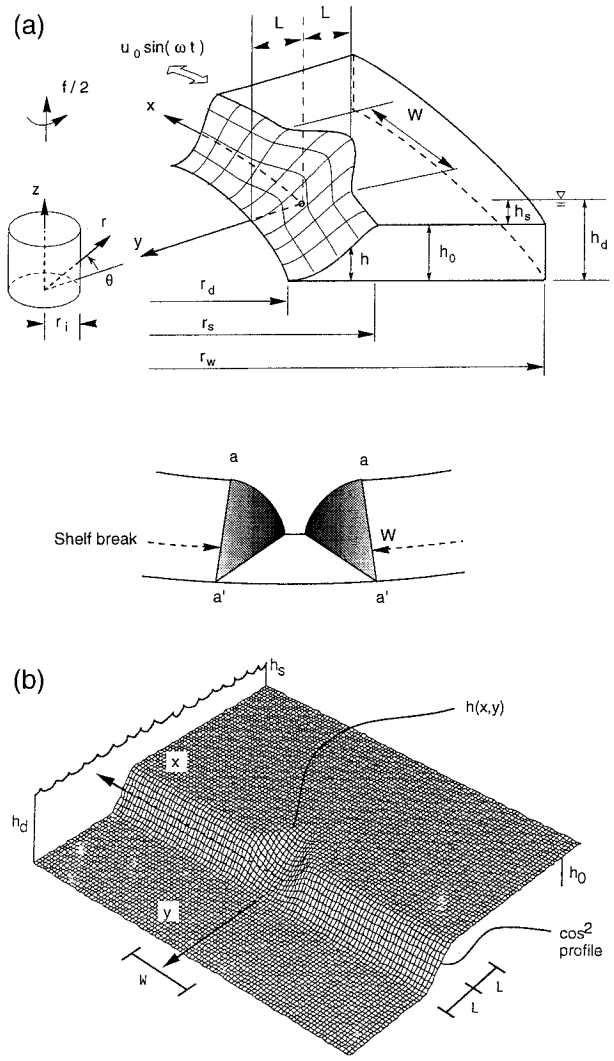

FIG. 1. Physical systems: (a) physical models and (b) numerical model. Note that the upper physical model schematic is for the ASU experiments; the canyon configuration is somewhat different for the LEGI model [see lower illustration in (a) and the text].

ties. The first is the 13-m diameter, 1.2-m-deep tank of the Laboratoire des Ecoulements Geophysiques et Industriels (LEGI), while the second is the 1.8-m diameter test cell of the Arizona State University (ASU). The larger tank is used because of the possibility of taking time series data using ultrasonic current meters, while the smaller tank is used because of its ease of usage and the capability of obtaining time line photographs (Lagrangian observations) of the motion fields. Because of the very large scale of the topographic feature used in the LEGI studies, the canyon geometry, while qualitatively similar to that used in the numerical experiments, was not precisely the same. Modern machining methods allowed for the topography used in the smaller ASU facility to closely approximate the model bathymetry used in the numerical studies, although a cylindrical geometry was used in the former and a rectangular one in the latter.

The physical models used for the LEGI and the ASU experiments are given schematically in Fig. 1a. The test cells are cylindrical tanks of radii r_w. Both of the tanks have central shafts of radii r_i. The shaft in the LEGI facility allows for the support of radial structures (pivoted on the shaft and mounted on rollers free to move along a rail along the tank periphery) upon which are mounted experimental instrumentation. In the ASU experiments, the shaft separates the working fluid from a laser scanner mounted along the test cell axis. It is assumed that the shafts in both of the facilities do not influence significantly the resulting motion fields. The cylindrical coordinate system (r, θ, z) is defined with the origin at the center of the test section floor and with $\theta = 0$ being along the axis of the canyon.

Axially symmetric shelf break models are placed along the periphery of the test cells; the model elevation profiles h(r) are defined as

$$h = \begin{cases} 0, & r < r_s - L \\ h_0 \cos^2 \dfrac{\pi(r_s - r)}{2L}, & r_s - L < r < r_s \\ h_0, & r_s < r < r_w, \end{cases} \quad (1)$$

where h_0 is the plateau height, r_s is the radial location of the beginning of the plateau (i.e., the shelf break), and $L = r_s - r_d$ is the width of the sloping region. In the LEGI model a canyon is introduced into the continuous shelf by first removing an azimuthal section of circumferential width W (the canyon width) measured along $r = r_s$; see the insert to Fig. 1a. The vertical sides of the shelf geometry aa′ are then ''smoothed'' by a cosine-squared shape having the same profile as given by (1); see the shaded regions on the insert of Fig. 1a. The portion of the canyon adjacent to the shelf is then formed by a plane surface sloping at 45° to the horizontal. The cross section of the ASU model continental shelf is also given by (1). The canyon used in the ASU geometry is the same shape as that used in the numerical experiments (with Cartesian coordinates appropriately adapted to cylindrical ones); see Figs. 1a,b and relation (4) below. The coordinates (x, y) are defined as the distances measured along the shelf break beginning at the canyon axis and normal to the shelf break, respectively (see Fig. 1a).

The test cells in both facilities are filled with water whose temperature, and hence density ρ and kinematic viscosity ν, is assumed constant. The acceleration due to gravity is taken as g. The test cells are then rotated at a constant anticlockwise angular velocity Ω_0 about a vertical axis until the water is spun up to solid body rotation. At equilibrium, the depth of the deep fluid as measured at $r = r_s - L$ is defined as h_d and that of the shallow fluid at $r = r_s$ as h_s. It is noted that the free surface has a parabolic shape whose depth in the LEGI facility for the Coriolis parameter $f = 2\Omega_0 = 0.25$ rad

s^{-1} leads to a surface elevation difference from the test cell center to its edge of 3.4 cm. The depth change from $r = r_s - L$ to $r = r_s$, however, is roughly only 0.4 cm in the present application. In the ASU facility, $f = 0.5$ rad s^{-1}, leading to a center to edge elevation difference of 0.3 cm and a corresponding depth change of 0.02 cm from $r = r_s - L$ to $r = r_s$. These surface level changes are much smaller than the fluid depth at $r = r_s$ and thus are considered negligible in both facilities.

To obtain alongshelf oscillatory motions, the turntable rotation rates, after solid body rotation has been reached, are made time dependent as given by

$$\Omega = \Omega_0 - \omega_0 \sin(\omega t),$$

where ω_0 and ω are the amplitude and frequency, respectively, of the modulation. Furthermore, $\omega_0 \ll \Omega_0$ so that the Coriolis parameter relative to an observer fixed to the turntable is approximately f. Relative to an observer on the turntable, the fluid thus oscillates in the azimuthal direction. We take as the characteristic oscillatory alongshelf velocity that background motion observed at $r = r_s$; that is,

$$u(t) = u_0 \sin(\omega t), \tag{2}$$

where $u(t)$ is the along-isobath background velocity and $u_0 = \omega_0 r_s$ is the amplitude of the oscillatory current. The objective is then to determine the motion field resulting from these along-isobath oscillations in the presence of the canyon topographic feature.

The methods of flow visualization employed included the introduction of (i) neutrally buoyant dye tracers (food coloring or fluorescent dye) into the flow field so as to form streak lines (e.g., see Fig. 4) or time lines (e.g., see Fig. 5), or (ii) free surface floats. Eulerian time series velocity data were taken in the LEGI experiments by employing ultrasonic current meters. Eight such current meters were used by locating them in straight-line patterns across the shelf break geometry. Measurements were typically taken for five oscillation periods of the background motion.

Typical experiments were initiated by first filling the tank to its desired level while the turntable was rotating. Several hours were allowed for the fluid to reach an approximate solid body rotation; this was checked by following radially oriented time lines to assure that secondary motions owing to large-scale eddying motions and surface wind effects were reduced to the extent possible. When the fluid had reached a satisfactory state of solid body rotation, the turntable modulation was initiated. Typically, ten oscillations were allowed prior to beginning velocity measurements.

It is straightforward to show that the characteristics of the resulting motion fields depend on the following dimensionless parameters:

$$\mathrm{Ro} = \frac{u_0}{fW}, \quad \text{Rossby number,}$$

$$\mathrm{Ro}_t = \frac{\omega}{f}, \quad \text{temporal Rossby number,}$$

$$E = \frac{\nu}{fh_s^2}, \quad \text{Ekman number,}$$

$$\mathrm{Fr} = \frac{f^2 L^2}{g h_s}, \quad \text{Froude number, and}$$

$$\frac{h_s}{h_d}, \quad \frac{h_s}{L}, \quad \frac{r_s}{r_w}, \quad \frac{L}{W}, \quad \frac{r_s}{L}, \quad \text{geometrical.}$$

It is also found convenient to define X as the normalized excursion amplitude of an undisturbed particle at the radial location r_s; thus

$$X = \frac{u_0}{\omega W} = \frac{\mathrm{Ro}}{\mathrm{Ro}_t}, \quad \text{normalized excursion amplitude.}$$

It is emphasized, however, that as indicated, X is not an independent parameter. The values (ranges) of the various dimensional and dimensionless parameters considered in the LEGI and ASU laboratory experiments and in the numerical model studies are given in Table 1. The parameter values for the specific experiments conducted in these studies are given in Tables 2, 3, and 4, respectively.

Extensive experimentation concerning wind stress effects along the free surface for both the LEGI and ASU facilities in the absence of a canyon has been conducted previously and reported in Zhang et al. (1996). These experiments were performed in the absence of turntable modulations for $f = 0.25$ and 0.5 rad s^{-1} for the LEGI and ASU facilities respectively; that is, the same background rotation rates as for the present experiments. The LEGI study showed a complex radial distribution of largely clockwise motions in the vicinity of the sloping region with a mean clockwise advection of roughly 0.1 cm s^{-1}; this compares with the typical range of forcing magnitudes of $u_0 \sim 1.5$–8.0 cm s^{-1} and rectified flow speeds in the same range. The ASU experiments showed a more regular radial distribution with a mean clockwise wind-driven motion of the order of 0.05 cm s^{-1}; this compares with $u_0 \sim 0.5$–4.0 cm s^{-1} and rectified flow speeds of similar magnitude. One should thus expect wind-forced mean motions of these small orders to be superimposed on any rectified flows observed in the presence of modulated alongshelf motions.

Experiments were also conducted to determine the motion field in the absence of a canyon for cases in which turntable modulations were being employed. Using the LEGI facility, six separate turntable frequency and amplitude modulations covering the range of these parameters considered in the canyon experiments were investigated. The hodographs (with mean components removed) of the horizontal velocity fields over the shelf,

TABLE 1. Parameters used in LEGI, ASU, and numerical experiments.

Parameter	Description	LEGI	ASU	Numerical
r_d	radius at slope edge	4.5 m	55 cm	—
r_s	radius at shelf break	5.0 m	65 cm	—
r_w	radius at tank wall	6.5 m	90 cm	—
r_i	radius of shaft	0.2 m	22.7 cm	—
h_s	fluid depth at shelf break	0.05 m	2.5 cm	0.05 m
h_d	fluid depth at slope edge	0.35 m	10.5 cm	0.35 m
L	canyon length	0.5 m	10 cm	0.5 m
W	canyon width	1.1 m	20 cm	1.0 m
u_0	characteristic background speed	1.6–7.8 cm s^{-1}	0.8–3.9 cm s^{-1}	0.9–3.9 cm s^{-1}
ω	flow oscillation frequency	0.025–0.35 rad s^{-1}	0.15–0.5 rad s^{-1}	0.06–0.25 rad s^{-1}
f	Coriolis parameter	0.25 rad s^{-1}	0.50 rad s^{-1}	0.25 rad s^{-1}
ν	kinematic viscosity	0.01 cm^2 s^{-1}	0.01 cm^2 s^{-1}	1.3 cm^2 s^{-1}
$\mathrm{Ro} = u_0/fW$	Rossby number	0.04–0.25	0.04–0.16	0.04–0.16
$\mathrm{Ro}_t = \omega/f$	temporal Rossby number	0.1–1.5	0.3–1.0	0.25–1.00
$E = \nu/fh_s^2$	Ekman number	$1.6(10)^{-3}$	$3.2\ (10)^{-3}$	—
$\mathrm{Fr} = f^2L^2/gh_s$	Froude number	0.03	0.01	—
h_s/h_d	geometrical	0.14	0.23	0.14
h_s/L	geometrical	0.10	0.25	0.10
r_s/r_w	geometrical	0.7	0.7	—
L/W	geometrical	0.45	0.50	0.50
r_s/L	geometrical	10.0	6.5	—

the sloping region, and the deep water demonstrated essentially an along-isobath motion. Weak cross-isobath or lateral motions could be observed over the shelf and over the more shallow portions of the sloping region. These cross-isobath motions were found to be consistent with interior return flows forced by bottom Ekman layer transports due to the oscillatory background flow. In light of these very weak cross-isobath motions and in keeping with previous studies of such flows for long ridges as discussed above (e.g., Zimmerman 1978), very weak residual along-isobath flows were expected for the no-canyon case. In fact, in all of these no-canyon experiments, wind effects dominated the residual motion field with the mean flow being clockwise (i.e., in the direction of the wind stress) at essentially all measurement locations and for all experimental parameters considered.

TABLE 2. LEGI experiments.

Experiment	Ro_t	Ro	X	Measurements	
				Downstream	Canyon
L1	0.1	0.05	0.51	x	
L2	0.2	0.05	0.26		
L3	0.5	0.05	0.10		
L4	0.8	0.05	0.06		
L5	1.0	0.05	0.05		
L6	0.1	0.10	1.00		
L7	0.2	0.10	0.50		
L8	0.5	0.10	0.20	x	x
L9	1.0	0.10	0.10		
L10	1.5	0.10	0.06	x	x
L11	0.5	0.15	0.30		
L12	0.2	0.20	1.00	x	
L13	0.8	0.20	0.25		
L14	0.5	0.25	0.50		

3. Physical model results

a. Flow regime diagram

The initial experiments with a canyon geometry were directed toward obtaining a flow regime diagram delineating the various characteristic flow types that would be observed for the ranges of the governing parameters considered in the LEGI and ASU experiments; see Tables 2 and 3. To this end it was assumed that the Ekman and Froude numbers in both experimental programs were sufficiently small so that these parameters were not of primary importance; see Table 1. Furthermore, the geometrical parameters were held constant and were approximately the same in the LEGI and ASU experiments, thus allowing one to investigate the dependence of the characteristic motion fields on the temporal Rossby and Rossby numbers alone. Characteristic flows were thus classified and delineated on a Ro_t against Ro flow regime diagram.

For the range of parameters investigated, two rather distinct flow types were observed. In the first, designated as the ''cyclone regime,'' prominent cyclonic eddies were formed and evolved during each cycle of the background flow as described below. In the second, termed the ''cyclone-free regime,'' no such cyclonic

TABLE 3. ASU experiments.

Experiment	Ro_t	Ro	X
A1	0.3	0.04	0.13
A2	0.5	0.04	0.08
A3	0.8	0.04	0.05
A4	1.0	0.04	0.04
A5	0.6	0.10	0.17
A6	0.3	0.16	0.52
A7	1.0	0.16	1.57

TABLE 4. Numerical experiments.

Run	Ro_t	Ro	X	$u_{max}(1)/u_0$	$y_{max}(1)/L$
N1 0.25	0.04	0.16	0.80	0.00	
N2 0.25	0.08	0.32	0.57	0.10	
N3 0.25	0.12	0.47	0.57	0.06	
N4 0.25	0.16	0.63	0.56	0.10	
N5 0.50	0.04	0.08	0.77	0.00	
N6 0.50	0.08	0.17	0.64	0.04	
N7 0.50	0.12	0.24	0.55	0.06	
N8 0.50	0.16	0.32	0.48	0.08	
N9 0.75	0.04	0.05	0.09	0.06	
N10	0.75	0.08	0.10	0.13	0.04
N11	0.75	0.12	0.16	0.91	0.08
N12	0.75	0.16	0.21	0.84	0.08
N13	1.00	0.04	0.04	0.03	0.10
N14	1.00	0.08	0.08	0.04	0.00
N15	1.00	0.12	0.12	0.08	0.00
N16	1.00	0.16	0.16	0.10	0.00

vortices were in evidence. These flow types are now described qualitatively and the experimental observations presented, which led to these classifications. A Ro_t against Ro flow regime diagram is given in Fig. 2, where the location of the respective symbols designates the parameter values at which the noted flow type was observed; the closed symbols represent LEGI experiments and the open symbols ASU runs. The dashed line represents the approximate boundary between the flow types.

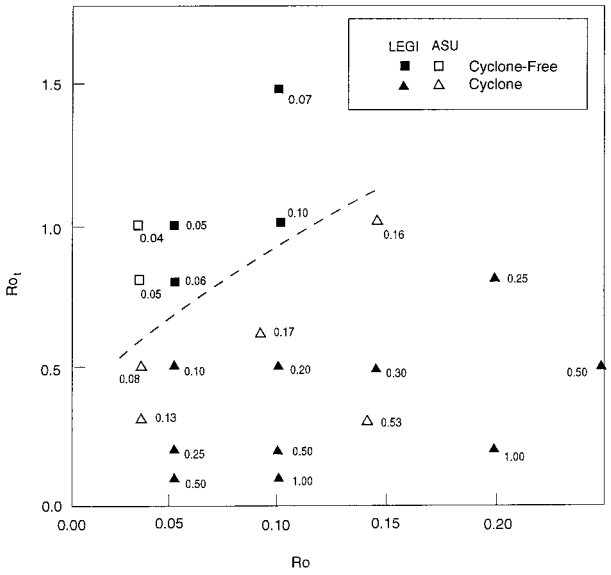

FIG. 2. Temporal Rossby number against Rossby number flow regime diagram. The dashed line is the approximate boundary between the cyclone and cyclone-free regimes. The numbers adjacent to the symbols represent the normalized excursion amplitudes X.

1) CYCLONE REGIME

The cyclone regime is observed at sufficiently small temporal Rossby numbers for all of the Rossby numbers investigated; as indicated by Fig. 2, the boundary between the cyclone and cyclone-free regimes is found at increasing Ro_t for increasing Ro. Figure 3 is a schematic diagram of the principal features of the large-scale motion field for the cyclone flow regime. In discussing flow types, it is convenient to consider specific phases in the oscillatory cycle of the background flow. To this end we define the phase sequence A, B, C, D, and E, where phase A refers to a flow at rest and about to begin moving from right to left and with each phase being separated by one-quarter cycle; see the insert of Fig. 3.

For the cyclone regime, one observes from the laboratory experiments (a numerical run for this flow type is discussed below) that, soon after the background motion moves from phase A toward B, a cyclonic eddy α begins to strengthen on the right side of the canyon interior; see Fig. 3a. This cyclone is driven by the tendency of the right to left flow to (i) separate from the topography owing to shear layer instability (e.g., as in the flow past a cylinder as discussed by Batchelor 1970) and (ii) have its vortex lines stretched as fluid parcels are advected over the plunging depth contours. Cyclone α is then observed to grow but remain roughly stationary during the period between phases A and C; note in Fig. 3 that cyclone α begins advecting toward the right between phases B and C. As cyclone α strengthens, fluid is advected from the deep water into the canyon and from left to right across the depth contours on the right side of the canyon interior. This process, in turn, forces fluid flowing from right to left across the shelf region to move toward the test cell boundary forming a ''jet-like'' motion, which is deflected anticyclonically over the shelf and around the canyon; see Fig. 3. As this jet then advects over the depth contours, its vortex lines are stretched leading to the formation of a second cyclonic vortex β in the approximate location indicated; β is initiated in the time interval between phase A and B.

As the background flow reverses at phase C, cyclone α advects around the right-hand corner of the canyon topography and moves toward the right and then ''downstream.'' Because of the large tidal excursions characteristic of this flow type and owing to the strong left to right rectified flow along the depth contours of the shelf break to the right of the canyon (see below), cyclone α advects downstream (i.e., to the right of the

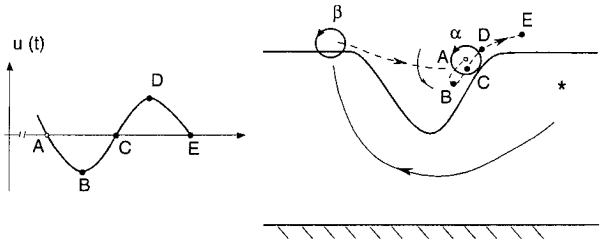

FIG. 3. Schematic diagram for the eddying motion for the cyclone flow regime. The insert defines the phases A–E in the oscillatory cycle of the background flow.

canyon) during the flow phases C to E; the rectified flow continues advecting α downstream where it eventually decays by Ekman suction. During this same period (i.e., from phase C to E), cyclone β moves across the canyon from left to right and by phase E is located at approximately the same location as occupied by cyclone α at the beginning of the cycle (i.e., phase A). This process continues periodically for each subsequent cycle of the background flow.

Figures 4a–c depict streakline photographs of dye tracers injected at mid depth on the shelf region at the two locations indicated by the arrows for a LEGI experiment in the cyclone regime; the dye tracers are continuously injected beginning at phase A, with the photographs taken at phases B, midway between B and C, and C, respectively. The inserts indicate the time in the flow cycle at which the respective photographs were taken as well as the total time (shaded region) for which the dye tracer has been injected. The outline of the canyon is as in Fig. 1a, and the background rotation is vertically upward.

Figure 4a shows clearly that a cyclonic eddy is located on the right side of the canyon; the path of the dye tracer moves to increasing fluid depths leading to vortex stretching and hence cyclonic vorticity production, as described above. Furthermore, the anticyclonic motion away from the canyon and on the shelf is apparent. Figure 4b shows the development of the cyclone on the sloping region to the left of the canyon as well as the further development of the cyclone on the right side of the canyon. Note that while the background motion is still from right to left in this phase, the dye tracer to the right of the canyon has begun to advect toward the right. This owes to the influence of the strong cyclonic structure that is active on the right side of the canyon interior. In Fig. 4c, one observes that the cyclone on the left, outside of the canyon, has begun to move to the right even though the background flow at this phase is at rest. This can be understood by employing the concepts of two possible mechnanisms. In the first, one can consider a mirror image vortex (an anticyclone) being placed along a radial line at a location outside the tank at a distance approximately the same as the distance from the ''real'' cyclone to the wall; for a straight wall it would be exactly the same distance. This mirror image in effect satisfies the zero normal velocity boundary condition for the vortex along the wall; see, for example, Prandtl and Tietjens (1934). The image vortex thus induces a left to right motion on the cyclone. The second contributing effect is that of a rectified (mean) left to right flow that occurs along the depth contours of the shelf and the canyon (see below). Note finally that by phase C, the cyclone that had been located on the right of the canyon interior has already advected to the right and out of the canyon.

Figures 5a–e are a time sequence of photographs and associated interpretive sketches of an experiment with the ASU facility also illustrating the cyclone flow regime. In this experiment radially oriented time lines λ_1 and λ_2 were established $\approx$1 cm below the free surface after the flow field had reached a periodic state; designate this time as $t = 0$ and the lines as $\lambda_1(0)$ and $\lambda_2(0)$, respectively. The illustrations are for flow phases A, B, C, D, and E, respectively, and were taken beginning at seven oscillation cycles after inserting the original time lines. The boundaries between the sloping region and deep water and shelf regions, respectively, are indicated by the dashed lines, with the canyon location specified by the U-shaped portion of the lower dashed line. The straight dashed line to the right of the illustrations is added to serve as a reference with which instantaneous locations of tonguelike dye tracers can be easily visualized. The radial time lines are Lagrangian indicators of flow patterns and, especially in unsteady flows, as being considered herein, care must be exercised in interpreting the observations.

The most obvious feature of the time line patterns is that a rectified flow along the shelf break depth contours occurs to the right, or downstream, of the canyon. Note that similar features are not found upstream of the canyon. Each tongue-shaped feature on the right side of the canyon is formed by the dye tracer emerging from the canyon region, which has been ''stirred'' in the canyon during each oscillation cycle. Each succeeding oscillation cycle finds the tips of the previous tongues having moved downstream, indicating the presence of a mean flow. Note that the tips of the tongues are found at different radial locations for different phases of the flow cycle, indicating the oscillatory nature of the radial velocity component as forced by the interaction of the alongshelf background flow with the canyon. Wind effects in both the deep and shallow water regions tend to drive the time lines in those areas from right to left. The time lines in the deep region also seem to be stirred into irregular patterns by the wind and other background currents in the tank.

Beginning with phase A (Fig. 5a), cyclonic structures α and β have been delineated on the interpretive sketches allowing one to follow their qualitative development and movement with time; these correspond qualitatively to the cyclonic eddies α and β, respectively, in Fig. 3. For example, β is very weak at phase A, strengthens through phase C, and is advected to the right interior wall of the canyon by phase E. Cyclone α, on the other hand, strengthens during the period from phases A to C and then is advected downstream during the period between phases C and E. These observations are in consonance with the qualitative discussion above concerning this flow type as observed in the LEGI experiments.

2) CYCLONE-FREE

For sufficiently large Ro_t and the range of Ro studied, there is no evidence of the formation of cyclones in either the canyon or to the left of the canyon, as described above. This owes to the fact that fluid parcels

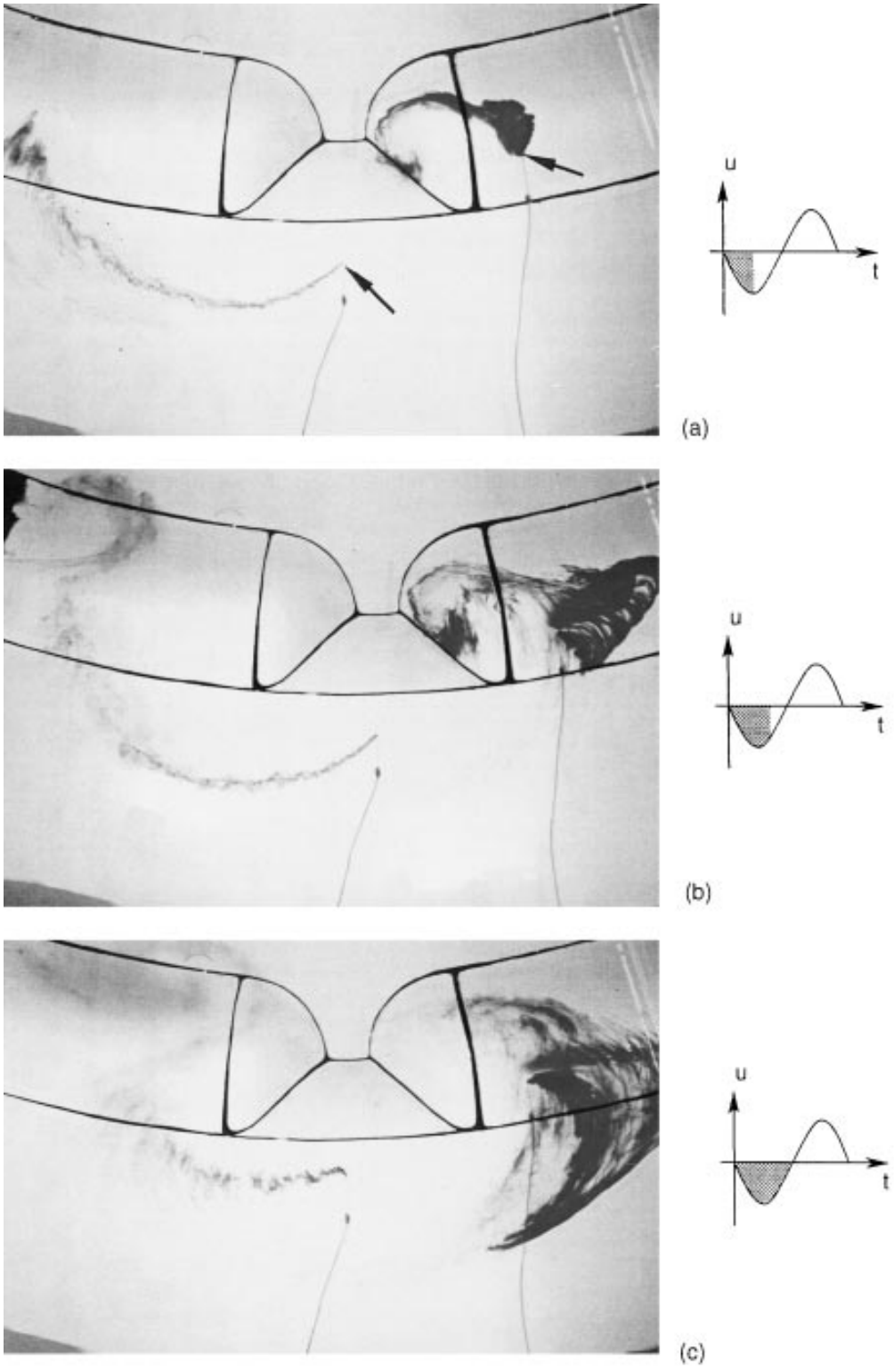

FIG. 4. Streaklines from the positions marked by arrows in (a) for a LEGI experiment in the cyclone regime for $Ro_t = 0.2$ and $Ro = 0.20$ (see experiment L12 in Table 2). The photographs were taken at phase B, midway between B and C, and at C, for (a), (b), and (c), respectively. The dashed lines on photograph (a) indicate the location of the shelf break.

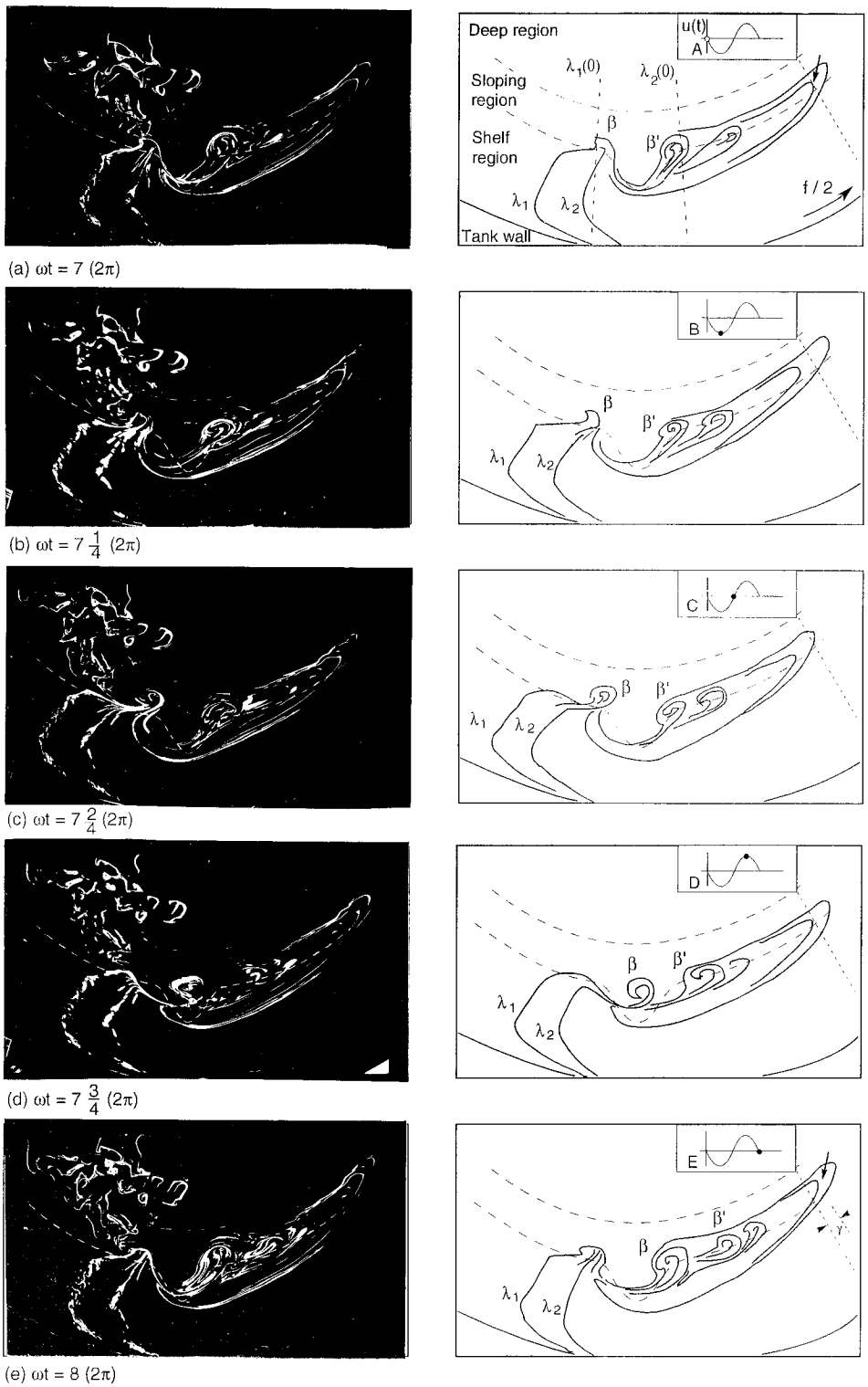

FIG. 5. Time line photographs and corresponding interpretive sketches for an ASU experiment in the cyclone regime: the parameter values are $Ro_t = 0.3$ and $Ro = 0.04$. The photographs were taken at phases A, B, C, D, and E for (a), (b), (c), (d), and (e), respectively. The time line was established at phase A seven cycles prior to the photograph of (a).

only move to small fractions of the characteristic canyon dimension so that closed eddies do not have time to form. Using time lines in the ASU experiments, one observed that the dye tracers oscillated back and forth along the depth contours both inside and external to the canyon region. No significant mean tracer displacements were observed. Because of the small normalized excursion amplitudes in these experiments, the nonlinear interaction between the background oscillatory currents and the canyon topography is weak, and the associated mean flows generated are weak as well. The numerical experiments predict that rectified flows do occur in the cyclone-free flow regime but that they are small and, in fact, comparable in magnitude to the oppositely directed, wind-driven currents. Hence, because of wind effects, the laboratory experiments cannot be used to accurately determine rectified velocities in the cyclone-free regime.

b. Eulerian time series measurements (LEGI)

Time series Eulerian data were taken in the LEGI experimental program using eight ultrasonic velocimeters. A description of these instruments and the techniques used to obtain velocity data in a horizontal plane are given in Zhang et al. (1996). The velocimeters were placed at various azimuthal locations at a depth of 2.5 cm below the free surface and at the radial locations indicated in Fig. 6a; starting on the shelf and ending in the deep water, these locations are designated as S1–S8, respectively. The azimuthal locations of various measurements are indicated in Fig. 6b. Locations over the canyon are designated as c1–c5, with c3 being along the canyon axis. Locations a0–a5 designate azimuthal positions external to the canyon. The numbers in parentheses below the azimuth designations indicate the number of characteristic canyon dimensions W from the canyon axis (c3) to the azimuth in question measured along the shelf break. Table 2 lists the parameter values for each of the experiments conducted in the LEGI program. In all of the experiments, measurements were taken at a0. For those studies indicated as ''canyon'' and ''downstream,'' measurements at c1–c5 and a0–a5, respectively, were also made.

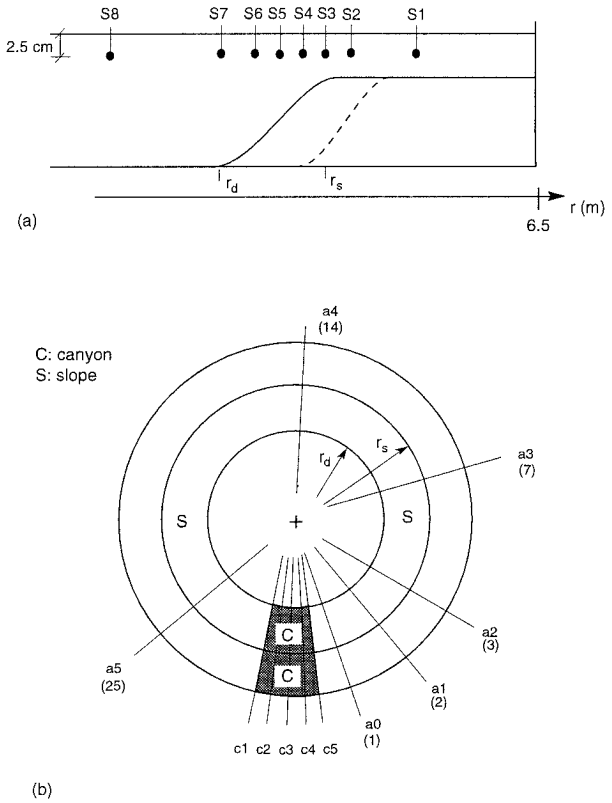

FIG. 6. Schematic representation of placement of velocimeters in LEGI experiments: (a) radial distribution and (b) azimuthal location of radial arrays. The designations c1–c5 and a0–a5 represent measurements within and external to the canyon, respectively. Note that the vertical and horizontal scales in (a) differ and that the radial measures in both (a) and (b) are not to scale.

1) HODOGRAPHS

Figure 7a presents a composite picture of hodographs obtained for one full oscillation cycle taken at various radial and azimuthal locations in the canyon region for an experiment for $\mathrm{Ro}_t = 0.5$ and $\mathrm{Ro} = 0.10$; that is, an experiment in the cyclone regime. The hodographs are obtained from the sum of the first three harmonic components with the mean flow being subtracted. The heavy dots indicate the center of each hodograph. The open circles, squares with asterisks and asterisks indicate phases A, B, and C, respectively, with phase A being the position in the oscillation cycle for which the flow is at rest and is about to move from right to left; the velocity scale is given in the lower right of the figure. Note first that the hodographs differ from ''regular'' tidal ellipses that are dominated by the fundamental harmonic component (see, e.g., the measurements far away from the canyon along a3 and a4 in Fig. 7b). Overall, the hodographs suggest that horizontal velocity gradients are important along both the left and right sides as well as the head and mouth of the canyon. These strong gradients indicate that the horizontal advection terms in the equations of motion are important, indicating the system is nonlinear in the canyon. The hodographs for positions within the canyon, as given in Fig. 7a, are consistent with the observations with dye tracers that the scale of the eddying motion is that of $W \sim L$; that is, the canyon width and length, respectively, which are both of the same order in the present study.

Figure 7b depicts hodographs for the same experiment as in Fig. 7a but at azimuthal locations a1–a5 (i.e., downstream of the canyon). One notes that the signals are more elliptical compared with their counterparts in the canyon region. This can be understood because the flow in the downstream region is more or less linear. The amplitude of the radial velocity component de-

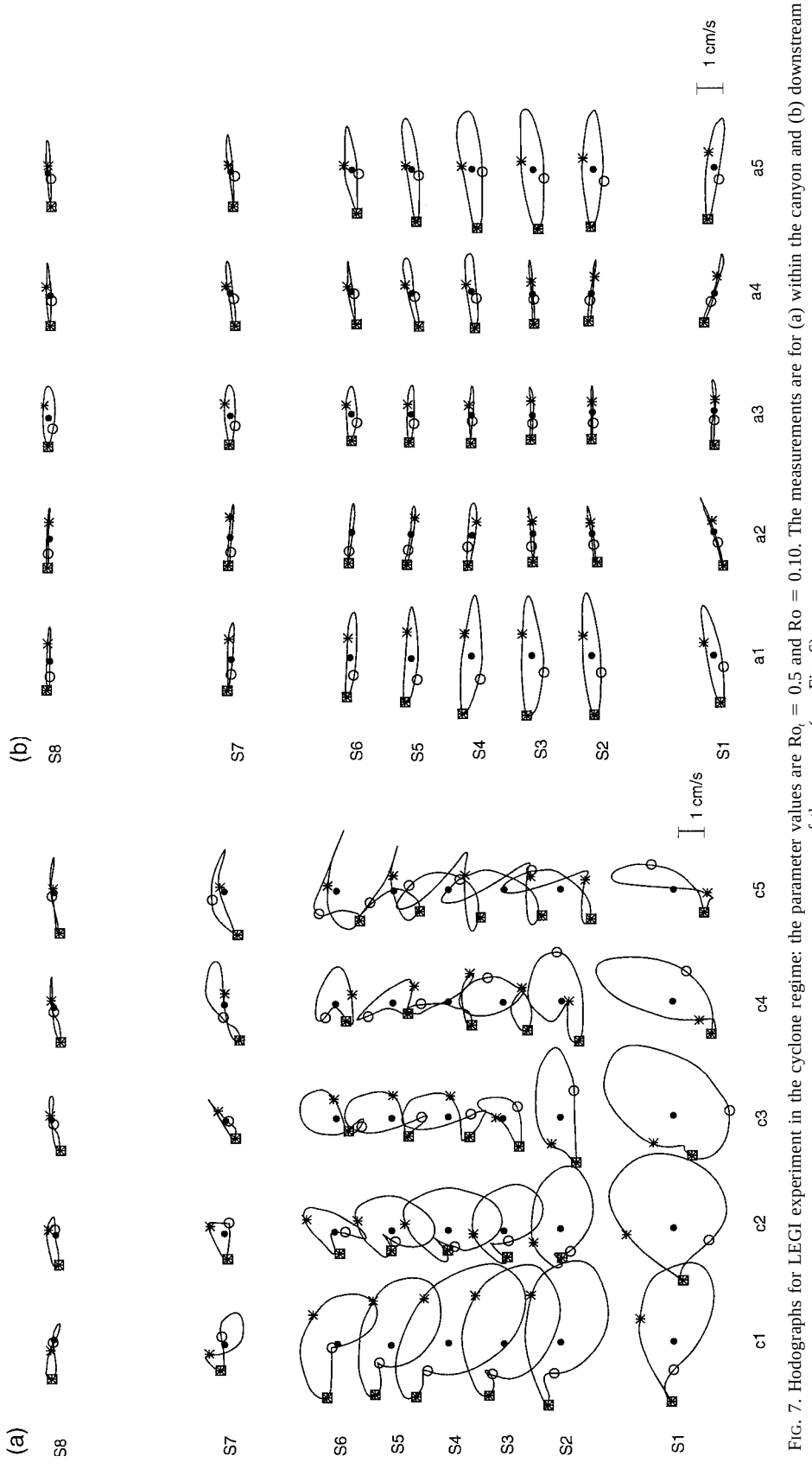

FIG. 7. Hodographs for LEGI experiment in the cyclone regime: the parameter values are $Ro_r = 0.5$ and $Ro = 0.10$. The measurements are for (a) within the canyon and (b) downstream of the canyon (see Fig. 6).

creases with increasing distance downstream. Note that the streamwise (i.e., x) locations of the positions a1–a5 are distorted for convenience in Fig. 7b; for the actual x locations, refer to Fig. 6.

2) RECTIFIED FLOWS

Figures 8a,b depict the mean flow measured at the same locations for the same experiment as that of Figs. 7a,b, respectively. The patterns in the canyon show clearly that a mean flow along the canyon walls is generated in the canyon with the maximum value found at the exit over the sloping region. One also notes the weak right to left flow in the deep water region, indicating the response to wind effects. The measurements downstream of the canyon suggest a rather broad mean flow along depth contours, which decreases with the downstream coordinate; see Fig. 8b.

The mean flow measurements in Fig. 8a allow one to determine if the flow in the canyon region at the measurement level of 2.5 cm below the free surface is nondivergent. To this end, consider the volume flux per unit depth through the control volume indicated by the dashed lines in Fig. 8a. Here the line along S1 is on the shallow region, while that along S7 is at the deep water edge of the canyon. The lines along c1 and c5 are along the left and right extremes of the canyon, respectively. Denoting Q_L, Q_R, Q_S, and Q_D as the volume fluxes per unit depth across the left, right, shallow, and deep sides of the control volume, respectively, and using the measured mean flows at various stations along the boundary, one obtains $Q_L = -61$ cm^2 s^{-1}, $Q_R = 160$ cm^2 s^{-1}, $Q_S = 34$ cm^2 s^{-1}, and $Q_D = -8$ cm^2 s^{-1}. Thus, the net volume flux through the sides of the control volume is 125 cm^2 s^{-1}; that is, the flow is horizontally divergent at this level.

If one assumes that the flow is depth independent and given by the measurements of Fig. 8a, one also determines that the flow through a control volume given by the lateral boundary indicated by the dashed lines, but now extending throughout the fluid depth, is also divergent; that is, one determines a net outward volume flux of 720 cm^3 s^{-1}. One possibility for accommodating this horizontal divergence could be a transport into the control volume through the Ekman layers along the lower bounding surface of the system. Using the net outflow obtained from the calculation for the total fluid depth (i.e., 720 cm^3 s^{-1}), one would require a cyclonic mean flow above the Ekman layers of the order of $\sim$10 cm s^{-1} along the entire control volume boundary to obtain a mass balance. Such large mean motions are not observed, and we thus conclude that the mean flow must be three-dimensional in the canyon.

Owing to the choice of the control volume in which the fluid depths are small for the c1, c5, and S1 portions, we further conclude that the net transport into the control volume takes place principally through the S7 portion of the boundary and presumably deep in the fluid; that is, there is a continuous flux of fluid in the upcanyon direction in the lower levels of the canyon mouth. Unfortunately, measurements at greater depths along S7 were not taken in the present study and we must leave this conclusion as a deduction rather than a firm observation.

In order to investigate the degree to which the various flows change with the system parameters, measurements of the mean flow along the azimuth a0 (i.e., one canyon width W downstream of the canyon axis) were made for each set of experimental parameters considered. The maximum value $\bar{u}_{\max}$ of the rectified velocity along a0 was then used as a measure of the strength of the mean flow generated; this maximum was typically, but not always, found at radial location S3, the shelf break. Figure 9 is a plot of the normalized maximum mean flow along a0, $\bar{u}_{\max}(1)/u_0$, against the temporal Rossby number Ro_t for various Rossby numbers Ro; here the numeral 1 refers to the normalized streamwise location $x^* = x/W = 1$ at which the measurements were taken. One notes an increase in $\bar{u}_{\max}(1)/u_0$ to values greater than unity with Ro_t for $\mathrm{Ro}_t \leq 0.5$ and then a decrease to roughly zero as Ro_t reaches superinertial values. Except for the measurements at $\mathrm{Ro}_t = 0.5$, the measured values of $\bar{u}_{\max}(1)/u_0$ are relatively insensitive to the value of the Rossby number. At $\mathrm{Ro}_t = 0.5$, the measurements indicate a strong dependence on Ro, with larger values for smaller Ro; more will be said on this aspect below.

In order to measure the decrease in the intensity with the downstream distance, measurements of $\bar{u}_{\max}/u_0$ were made for four sets of parameters (see Table 3) at each azimuthal location a0–a5. These data are plotted on the $\bar{u}_{\max}/u_0$ against $x^* = x/D$ diagram of Fig. 10, where $x^* = 0$ represents the location of the axis of the canyon. The $\mathrm{Ro}_t = 1.5$ experiment is such as to generate essentially a zero mean flow. The $\mathrm{Ro}_t = 0.2$, Ro = 0.20 experiment shows that the maximum occurs downstream of a0 (i.e., $x^* = 1.0$). For the $\mathrm{Ro}_t = 0.1$, Ro = 0.05 and $\mathrm{Ro}_t = 0.5$, Ro = 0.10 experiments, the maximum $\bar{u}_{\max}/u_0$ occurs at or to the left of $x^* = 1.0$. The measurements show that the mean flow intensity, as indicated by the observable $\bar{u}_{\max}/u_0$, eventually decreases with the downstream coordinate. The decay owes to complex processes involving lateral friction and Ekman suction with the latter believed to be dominant in the laboratory experiments. The early theory of Greenspan and Howard (1963) shows the effectiveness of Ekman suction compared to lateral friction in the decay of vertical vorticity in rotating fluids. The Ekman suction process is undoubtedly important in effecting the decay of the vorticity of the rectified ''jet'' as it advects downstream; see also Pedlosky (1979).

c. Lagrangian displacement measurements (ASU)

The time line data taken in the ASU facility can be used to track the leading edge of the dye tracer tongue

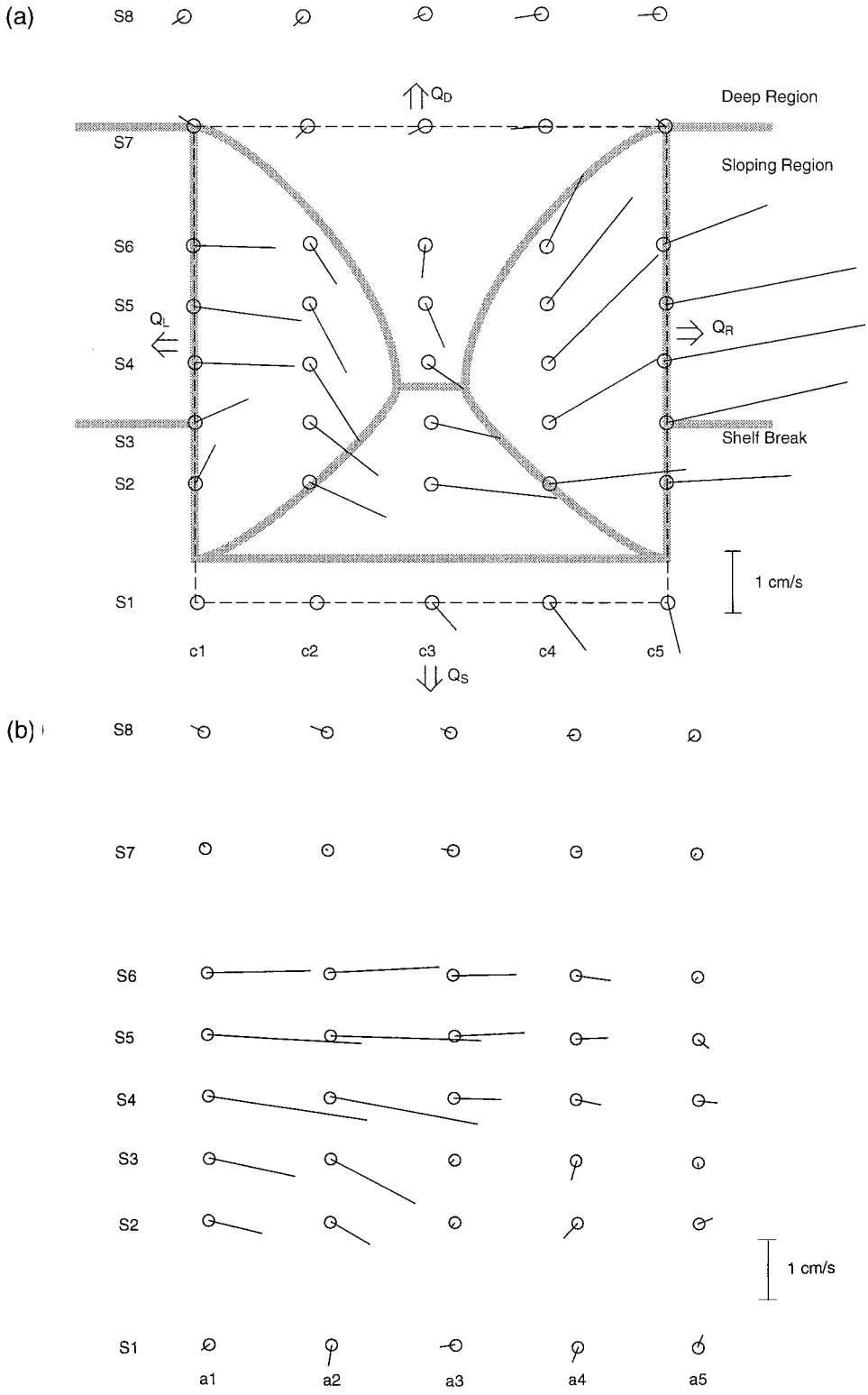

FIG. 8. Mean flow measurements for the same LEGI experiment as in Fig. 7 within the canyon (a) and downstream of the canyon (b). The wide shaded lines in (a) indicate the canyon boundaries as shown in Fig. 1a; the dashed lines are the boundaries of the control volume (see text).

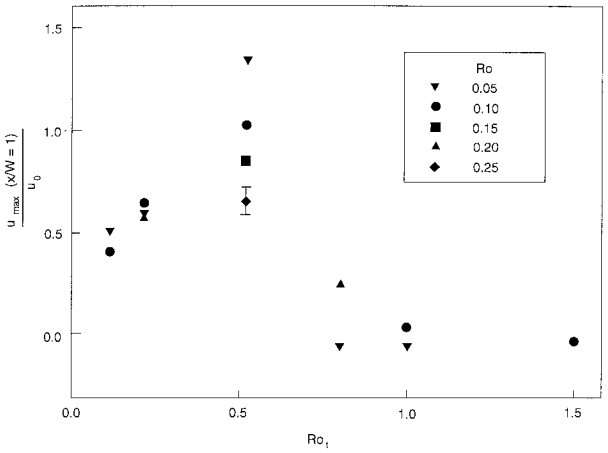

FIG. 9. Plot of normalized maximum rectified velocity measured at the streamwise location $x^* = x/W = 1$ against the temporal Rossby number for various Rossby numbers.

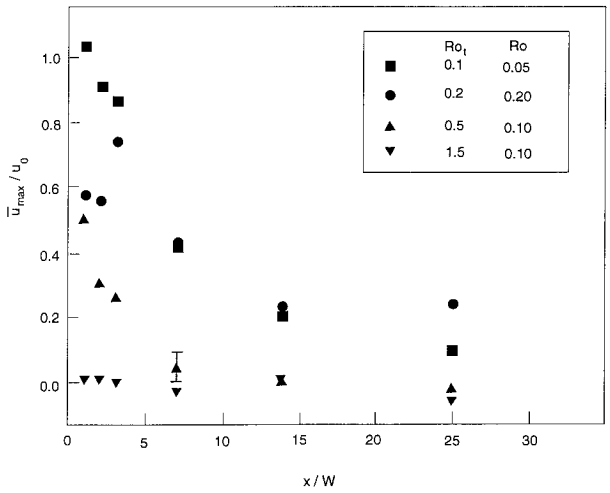

FIG. 10. Plot of normalized maximum rectified velocity against the normalized streamwise location for various temporal Rossby and Rossby number combinations.

as given, for example, by Figs. 5a–e. This leads to a determination of the maximum Lagrangian streamwise velocity as a function of the streamwise coordinate. One first identifies a given tongue as exemplified by the one noted by the arrow on the right side of Fig. 5a. The location along $r = r_s$ from the canyon axis is then designated as the coordinate x. This tonguelike feature is then tracked through one full oscillation cycle and the maximum streamwise displacement during one cycle γ determined; see the arrow on the right side of Fig. 5e. It is noted that while the present measurements were obtained starting with phase A (i.e., Figs. 5a–e), similar measurements starting with phase C were also made and the results, within experimental error, were the same.

Figure 11 depicts the normalized maximum time line displacement γ/Tu_0, where $T = 2\pi/\omega$ is the oscillation period, versus the normalized downstream distance x^* for an experiment at $Ro_t = 0.3$ and $Ro = 0.04$; that is, the same experiment as for Figs. 5a–e. Note that the normalized maximum time line displacement decreases with increasing x^*. This is in qualitative agreement with expectations based on the Eulerian mean flow measurements in the LEGI experiments. Unfortunately, quantitative comparisons between the Eulerian measurements (LEGI) and the Lagrangian measurements (ASU) could not be made owing to the fact that neither facility could be utilized to accurately obtain both Eulerian and Lagrangian velocity fields. It is also noted that such residual flows were found persistent over large distances downstream of the canyon. For example, under the same experimental conditions as for Fig. 11, $\gamma/Tu_0 \approx 0.06$ for $x^* \approx 10$.

4. Numerical model

The numerical model, rather than utilizing the cylindrical geometry of the physical model, employed a channel geometry. The numerical experiments used the smooth canyon geometry considered in the ASU experiments. Figure 1b is a sketch of the ocean floor bathymetry used in the numerical model, where the shelf break contour profile for $|x| \geq W/2$ is given by

$$h = \begin{cases} h_0, & y \leq 0 \\ h_0 \cos^2 \dfrac{\pi y}{2L}, & 0 \leq y \leq L \\ 0, & y \geq L, \end{cases} \tag{3}$$

and the origin of the coordinate system (x, y, z) is located directly below the shelf break at the elevation of the floor of the deep water region and centered in the streamwise direction of the canyon; see Fig. 1b. The depth contours in the canyon region defined by $-W/2 \leq x \leq W/2$, $0 \leq y \leq L$; $-W/2 \leq x \leq 0$, $-x - L \leq y \leq 0$; $0 \leq x \leq W/2$, $x - L \leq y \leq 0$ are given by

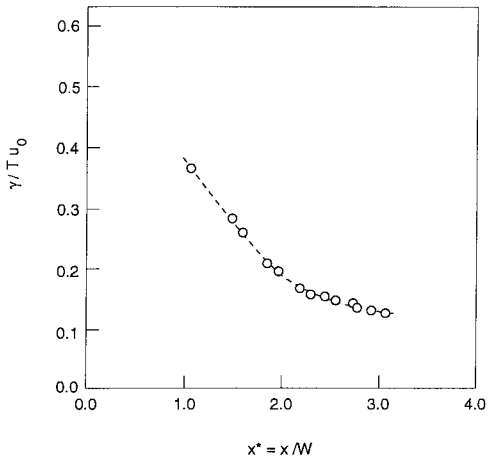

FIG. 11. Plot of the normalized maximum Lagrangian displacement of the leading edge of an advecting tongue formed by a cross-isobath time line against the normalized streamwise location (see text).

$$h = h_0 \cos^2\left[\frac{\pi}{2}\left(\frac{\frac{y}{L} + \cos^2\frac{\pi x}{W}}{1 + \cos^2\frac{\pi x}{W}}\right)\right], \quad (4)$$

so that the characteristic width and length scales of the canyon are W and L, respectively, as for the physical models.

The numerical model itself is essentially the same as that used in Verron et al. (1995). The model is the tridimensional primitive equation model given by Haidvogel et al. (1991) written in a channel configuration. The model employs the Navier–Stokes equations for a rotating fluid and uses the hydrostatic, Boussinesq, and incompressibility approximations. Furthermore, a rigid lid is used to filter external gravity waves. This approximation is justified owing to the small Froude numbers being considered and saves substantial computing time. Note that the rigid-lid approximation does not preclude horizontal pressure gradients and thus is still able to simulate free-surface slopes through differential pressure over the lid.

The governing equations for the model are the (x, y) momentum equations, the hydrostatic relation, and the relation for conservation of mass, which can be written, respectively, as

$$\frac{\partial u}{\partial t} + \bar{\mathbf{v}}\cdot\nabla u - fv = -\frac{\partial \Phi}{\partial x} + \Gamma_x, \quad (5a)$$

$$\frac{\partial v}{\partial t} + \bar{\mathbf{v}}\cdot\nabla v - fu = -\frac{\partial \Phi}{\partial y} + \Gamma_y, \quad (5b)$$

$$\frac{\partial \Phi}{\partial z} = -g, \quad (5c)$$

$$\frac{\partial u}{\partial x} + \frac{\partial v}{\partial y} + \frac{\partial w}{\partial z} = 0, \quad (5d)$$

where (u, v, w) are the (x, y, z) components of the velocity, $\nabla = (\partial/\partial x, \partial/\partial y, \partial/\partial z)$, Φ is the dynamic pressure, and Γ_x and Γ_y include both the forcing and dissipation terms. Horizontal dissipation effects are modeled by a harmonic term for the inner fluid (Laplacian lateral friction) and vertical friction effects are ignored. The former are included to provide numerical stability, while the latter assumption allows one to ignore bottom Ekman layer effects, which would have required a finer vertical resolution and hence increased computer time. The general hypothesis is that the principal mechanism of the rectification process owes to topographic effects of the canyon; furthermore, the friction required for the rectification is that introduced in the horizontal. The good qualitative agreement between the laboratory observations and the numerical model results in the vicinity of the canyon region (see Fig. 17 below) supports these hypotheses. On the other hand, Ekman suction is believed to be important in the downstream regions in the physical experiments and, thus, discrepancies might be expected between the numerical runs and laboratory experiments downstream of the canyon.

The set of equations (5a)–(5d) is solved using a finite-difference technique for the transformed, orthogonal, curvilinear coordinates in the horizontal plane. In the vertical, a σ-coordinate transformation, $\sigma = 1 + 2z/(h_d - h)$, is used. Owing to the neglect of bottom friction, the problem is reduced to solving for the depth-integrated flow over the vertical. A trapezoidal-leapfrog, time-stepping method is used for the temporal scheme.

Slip boundary conditions are applied along both lateral walls; not accounting for the presence of viscous boundary layers allows one to avoid grid refinement along these walls and the associated increased computational costs. As noted above for the physical model experiments, the canyon has a substantial effect on the overall flow for many characteristic canyon horizontal length scales downstream (i.e., $x > 0$) of the disruption in the shelf-break geometry. This ''long-range effect'' of the canyon produced difficulties in the numerical model in the sense of how to handle the ''upstream'' and ''downstream'' boundary conditions. Three approaches were used. The first employed periodic boundary conditions with a relatively short channel. This approach was used before it was clear that the canyon would have such an important effect far downstream. The approach failed since the overall flow field was a strong function of the channel length chosen, even for relatively long channels.

The second approach was to employ open boundary conditions, which had worked well on other problems using this code; see, for example, Nguyen and Verron (1995). This approach also failed for the present problem, however, because the forcing flow was purely oscillatory with no mean advection. The third approach, which led to the solutions presented herein, was somewhat of a combination of the above approaches. The procedure was to take a rather long channel and to apply periodic boundary conditions. But in addition, in the last half of the channel, the viscosity was increased by a factor of 10 from what it was in the first half; that is, a sponge layer was introduced. This procedure damped propagating disturbances far downstream of the canyon, making the perturbations negligible by the end of the channel and hence not introducing strong disturbances at the upstream edge of the flow region. The periodic boundary condition used thus did not seriously contaminate the incident periodic upstream flow. For the cases investigated and delineated in Table 4, we concluded that a channel of 15-m length was sufficient to obtain satisfactory results with this approach.

For experiment N12 in Table 4, experiments were conducted with (i) no sponge layer, (ii) a sponge layer in the last half of the channel, and (iii) a sponge layer in the last one-fifth of the channel. The downstream mean flow in roughly the first half of the channel was

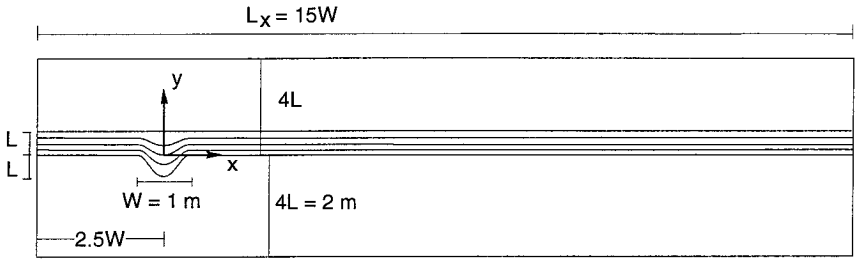

FIG. 12. Schematic diagram of the integration region for the numerical model. The light solid lines indicate the location of the sloping regions, with the canyon being on the left side of the figure.

essentially the same for all three cases. There were, of course, differences between the cases in the last half of the channel, with the no sponge experiment leading to an unacceptable mean flow at the channel entrance (exit).

A lateral viscosity A_h is required in the model for filtering the subgrid scales that, in turn, is needed for numerical stability reasons. The value of A_h chosen was 1.3×10^{-4} m^2 s^{-1} leading to a horizontal ''numerical'' Ekman number

$$E_h = \frac{A_h}{fD^2} = 5.3 \times 10^{-4}.$$

This choice was a compromise between having the finest possible grid resolution (and the related smallest possible lateral viscosity required for stability) in relation to the available computational capabilities. This value of the turbulent viscosity A_h used in the model is considerably larger than the kinematic viscosity of water, thus leading to a much larger horizontal Ekman number than for the laboratory experiments.

The domain used for the numerical model is sketched in Fig. 12. The portion with the narrowly spaced horizontal lines indicates the location of the sloping region with the deep water above and the shallow below. Note the location of the canyon to the left of the illustration. The streamwise and lateral dimensions of the model used were $L_x = 15W$ (15 m) and $L_y = 8L$ (4 m), respectively. The origin of the coordinate system (i.e., the axis of the canyon) was located $2.5W$ from the left boundary of the region and centered in the lateral direction. While the required horizontal resolution depends on the value of A_h used, for that value noted above it was found that a grid of 290 points in the longitudinal direction and 65 points in the transverse direction was adequate. The grid utilized in the y direction was not a regular one in that finer resolution was used in the shelf break and canyon regions. The grid interval in the x direction was regular with a value of $15/290 \approx 0.05$ m; an average interval in the y direction was $4/65 \approx 0.06$ m.

5. Numerical model results

We have investigated 16 sets of governing parameters in the numerical experiments as listed in Table 4. In order to compare the time-dependent nature of the numerical experiments with the corresponding observations in the physical experiments, a numerical run for a set of parameters in the cyclone regime (see Fig. 2) was conducted. Figures 13a–e depict the time-dependent vorticity fields for experiment N12 (see Table 4) for one period, 30 periods after starting the integration; the parameter values are $\mathrm{Ro}_t = 0.75$ and $\mathrm{Ro} = 0.16$ and solid contours correspond to cyclonic vorticity and dashed ones to anticyclonic vorticity. The location of the canyon in the various numerical run illustrations is indicated by the horizontal and vertical marks on the left side of the uppermost figure. In examining Fig. 13, it must be noted that the contour intervals are not the same for each of the illustrations.

One notes first that the cyclonic eddies are much stronger than the anticyclonic ones and seem to dominate the flow field as they did for the physical model experiments as exemplified by Figs. 4a–c and 5a–e; that is, the maximum cyclonic vorticity is roughly one order of magnitude larger than that of the anticyclonic vorticity at all phases of the flow cycle. For ease of following the movement of the various cyclonic eddies, they have been labeled α, β, γ, and δ on Figs. 13a–e; that is, from the oldest to the youngest, respectively. Looking first at the older eddies α and β, one notes that these have exited the canyon region and are being advected downstream while at the same time decaying. Cyclone γ begins at phase A on the right side interior wall of the canyon, strengthens during the period between phases A to C and then is advected to the right of the canyon during the period between phases C to D. Cyclone δ is formed to the left of the canyon between phases A and B, although some evidence of its presence is already indicated at phase A. This cyclonic structure strengthens until phase C and then is advected to the right side of the canyon interior; by phase E it assumes roughly the same position as γ had at phase A of this same cycle. These results for the numerical model are in close qualitative accord with the observations of the physical models for experiments in the same flow regime (i.e., Figs. 4a–c and 5a–e).

Figures 14a–c show a set of results for the time-mean streamfunction, vorticity, and velocity vector distribu-

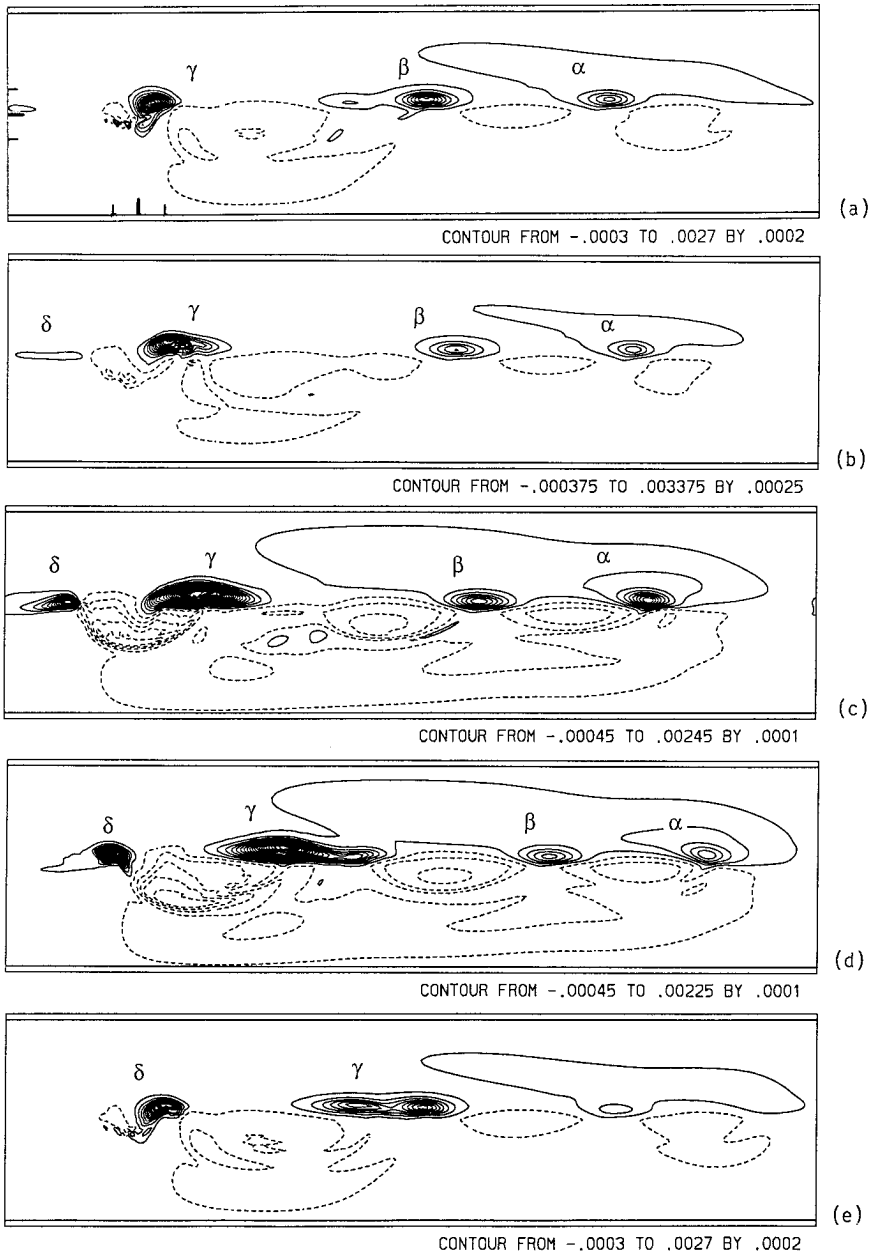

FIG. 13. Plots of the time-dependent vorticity field from the numerical model for experiment N12 of Table 4: that is, $Ro_t = 0.75$, $Ro = 0.16$. The integration was started 30 periods prior to the illustrations and the phases represented are A, B, C, D, and E for (a), (b), (c), (d), and (e), respectively. Solid contours represent cyclonic vorticity and dashed ones, anticyclonic. The outer boundaries of the canyon are indicated by the markings near the left of (a). The contour interval and range for (a) is $2.0(10)^{-4}$ s^{-1} and $-3.0(10)^{-4}$ to $27.0(10)^{-4}$ s^{-1}, (b) $2.5(10)^{-4}$ s^{-1} and $-3.75(10)^{-4}$ to $33.75(10)^{-4}$ s^{-1}, (c) $1.0(10)^{-4}$ s^{-1} and $-4.5(10)^{-4}$ to $24.5(10)^{-4}$ s^{-1}, (d) $1.0(10)^{-4}$ s^{-1} and $-4.5(10)^{-4}$ to $22.5(10)^{-4}$ s^{-1}, and (e) $2.0(10)^{-4}$ s^{-1} and $-3.0(10)^{-4}$ to $27.0(10)^{-4}$ s^{-1}.

tion for a typical experiment; that is, run N1 from Table 4. This experiment is characteristic of the qualitative nature of all of the experiments conducted. Focusing, for example, on the time-mean velocity vector pattern depicted in Fig. 14c, one notes that a rectified flow, whose principal direction is along the shelf break with the shelf on the right facing downstream, is generated in the vicinity of the canyon. This rectified flow has a mean direction that generally follows the depth contours of the canyon, finally leading to a more or less rectilinear flow, parallel to and centered on, the shelf break downstream of the canyon. The mean flow pattern corresponds to a succession of alternating eddies, positive, negative, and positive, over the canyon region. It is

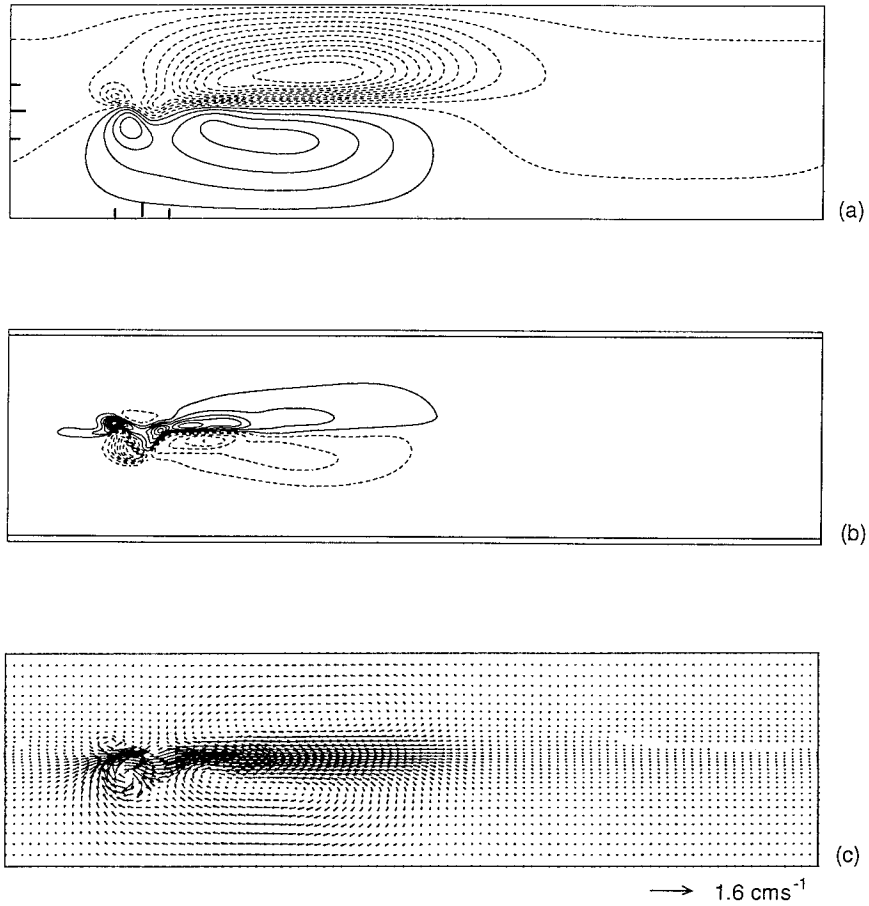

FIG. 14. Plots of the mean (a) streamfunction, (b) vorticity, and (c) velocity field obtained from the numerical model for $Ro_t = 0.25$ and $Ro = 0.04$. The outer boundaries of the canyon are indicated by the markings near the left of (a). The contour interval for (a) is 0.5 cm^2 s^{-1}, with the contours ranging from -5.75 to 2.25 cm^2 s^{-1}; for (b) the contour interval is $0.25(10)^{-4}$ s^{-1}, with the contours ranging from $-1.875(10)^{-4}$ to $2.375(10)^{-4}$ s^{-1}. Dashed contours represent negative values.

observed that the intensities of these eddies and their precise locations are a function of the governing parameters. One dramatic effect of the canyon is that the rectified flow continues for many characteristic canyon length scales downstream of the canyon itself.

Figures 15a–d are plots of the mean velocity vector patterns for a fixed Rossby number $Ro = 0.08$ and a sequence of increasing temporal Rossby numbers Ro_t. These figures illustrate the substantial effect Ro_t plays on the downstream distance to which a significant rectified flow is observed; that is, the rectified flow speed at a given streamwise location decreases dramatically with increasing Ro_t. Care must be exercised in interpreting these illustrations because the velocity scale differs for each figure. Figures 15a–d show that while the qualitative nature of the mean flow patterns are similar in the various cases, quantitative values of the rectified flows vary significantly with Ro_t. The variation of such rectified flow patterns with Ro at fixed Ro_t do not generally exhibit such dramatic changes.

Perhaps the most important observation in the present physical and numerical model experiments is the existence of this downstream current along the shelf break, which can be significant far from the canyon region. Figure 16 illustrates the velocity profiles of the mean flow across the shelf break region at the normalized streamwise location $x^* = x/W = 1.0$ (i.e., near the canyon) for the same experiments as given in Figs. 15a–d. One's intuition would certainly suggest that the strongest rectified flows close to the canyon would lead to those flows that have the most significant mean velocities far downstream and this is clearly borne out by comparing Fig. 16 with Figs. 15a–d. The rectified velocity profiles also clearly show that the most intense current is centered on the shelf break (vertical dashed line) and that the current is not very strong far from the break; that is, on the shelf away from the break, above the deeper regions of the continental slope, and in the deep water region. Let us define the maximum value of the mean flow velocity obtained at $x^* = 1$ as $\bar{u}_{max}(1)/u_0$.

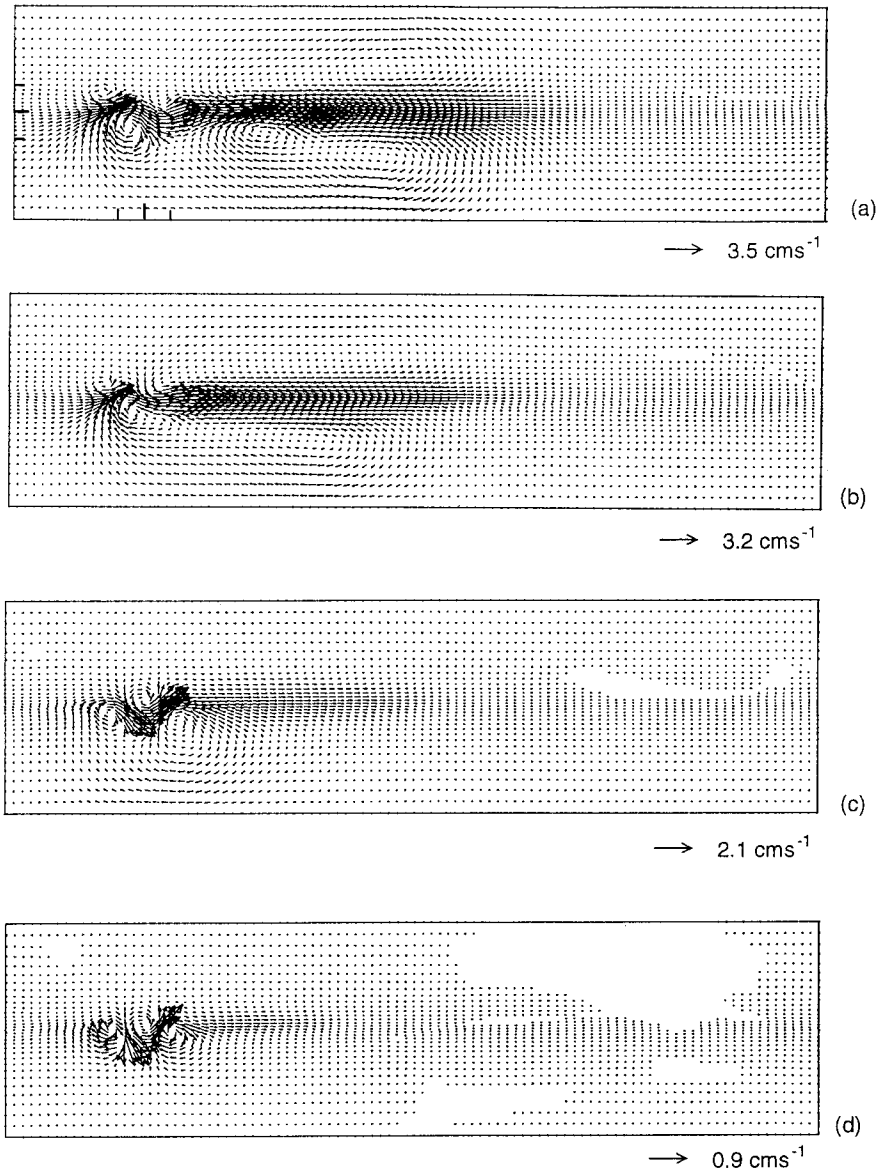

FIG. 15. Sequence of mean velocity fields for a fixed Ro = 0.08 and for Ro_t values of (a) 0.25, (b) 0.50, (c) 0.75, and (d) 1.00 The outer boundaries of the canyon are indicated by the markings near the left of (a). Note that the velocity scale is different for each plot.

Table 4 then gives the normalized lateral location of this maximum $y_{max}(1)/L$ for the various numerical experiments. As can be seen clearly, $\bar{u}_{max}(1)/u_0$ is found along the shelf break, or slightly to the deep water side of the break, for all of the experiments.

A horizontal width scale for the rectified current based on an *e*-folding factor is something like the canyon length scale L. Additionally, it can be noted from Fig. 16 that the rectified current width scale for a fixed Rossby number depends on the value of the temporal Rossby number. This owes to the fact that lateral disturbances to the background flow due to the canyon decrease with increasing Ro_t, leading to rectified flows whose characteristic horizontal length scales also decrease with increasing Ro_t. Note also that a small transverse asymmetry in the velocity profiles develops with increasing Ro_t.

One can compare the strengths of the rectified flows generated as a function of the system parameters by considering the variation of the normalized maximum mean velocity $\bar{u}_{max}(1)/u_0$. To this end, Fig. 17 is a plot of $\bar{u}_{max}(1)/u_0$ against the normalized excursion amplitude X for all of the numerical experiments (open symbols). Also plotted in Fig. 17 are the similar data from the LEGI physical model experiments as obtained from Fig. 9 (closed symbols). It must again be emphasized that

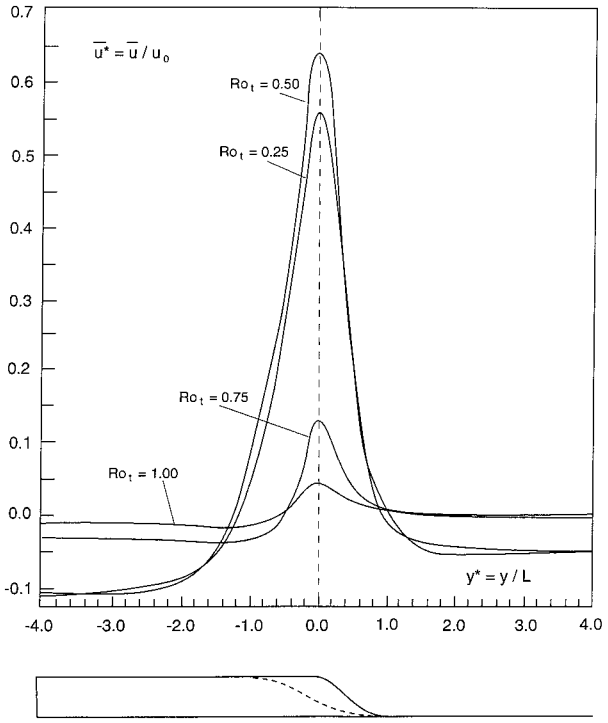

FIG. 16. Normalized along-isobath mean velocity profiles for the streamwise location $x^* = 1$ for Ro = 0.08 and a range of Ro$_t$; that is, for the same experiments as illustrated in Figs. 15a–d.

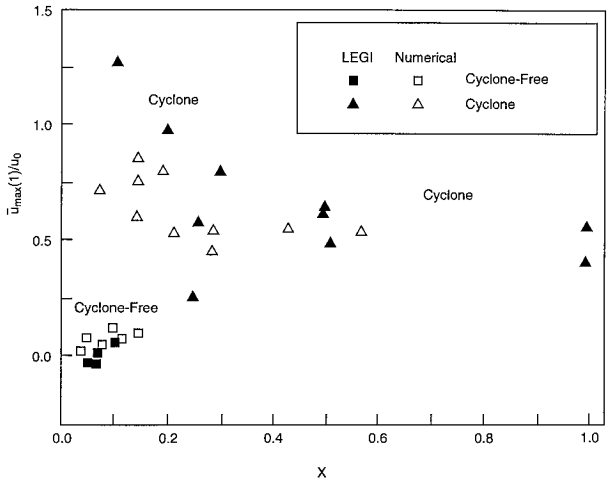

FIG. 17. Plot of the normalized maximum mean velocity obtained at $x^* = 1$ against the normalized tidal excursion; open symbols indicate numerical runs and closed symbols LEGI physical model experiments.

the actual canyon topography is different in the physical and the numerical models. Moreover, the mean flows in the numerical experiments were integrated over the depth, while the mean flows in the LEGI physical model experiments were measured at a single vertical position.

Both the physical and numerical model experiments in Fig. 17 indicate a similar behavior. For tidal excursions $X \leq 0.4$, the data collapse, showing a maximum rectified velocity at this location of the order of the mean forcing speed and independent of the specific values of Ro$_t$ and Ro; that is, $\bar{u}_{max}(1)/u_0 \sim 0.6$. Note that in the flow regime diagram of Fig. 2, radial lines represent lines of constant X, with X increasing with decreasing slope. Thus, for large X in Fig. 2, all of the experiments lie in the cyclone regime and lead to the observed roughly constant $\bar{u}_{max}(1)/u_0 \sim 0.6$ in Fig. 17.

For $X \geq 0.4$, the mean flow behavior has two branches, corresponding to the radial lines for smaller X in Fig. 2 crossing two flow regimes. For the lower branch, $\bar{u}_{max}(1)/u_0 \leq 1$, the general values increase with increasing X with all of the experiments being in the cyclone-free regime. For the upper branch, on the other hand, $\bar{u}_{max}(1)/u_0 \geq 1$, the normalized mean flow decreases with increasing X, with the experiments being in the cyclone regime; see also Fig. 2. The branching of the data in Fig. 17 recognizes that, in fact, this observable depends on two parameters, not just the normalized excursion amplitude X.

6. Relation of present findings to oceanic observations and models of others

In spite of the fact that the present study was not directed toward the modeling of a particular geographical location, one can note certain similarities between the present laboratory and numerical model experiments and oceanic observations. Because stratification was ignored in the present study, the observations of, for example, Hunkins (1988) and Hickey (1996), that the flow near the ocean surface is not influenced by the presence of the canyon, was not observed. One must thus consider oceanic observations at levels just above or within the canyon to make comparisons and, additionally, to realize that only qualitative comparisons can be made owing to the fact that (i) the oceanic measurements were made only at limited numbers of points in space and time and that many physical processes were occurring simultaneously and (ii) that the geometry and forcing in the laboratory and present numerics were highly idealized and did not correspond to any particular oceanic case. Nevertheless, some interesting comparisons can be made.

First, the observation of Hickey (1997) that local cyclonic vorticity on the upwind side of the canyon below the rim was observed in the early phases of the upwelling-favorable wind process has its counterpart in the cyclonic eddy observed to be shed on the right of the canyon in the right to left phase of the cyclone regime; see, for example, Figs. 3, 4, and 5. Durrieu de Madron (1994) also observed cyclonic vorticity on the upstream side of the canyon in this general region. We recall from Fig. 2 that the cyclone regime occurs at small temporal Rossby numbers, which, in turn, corresponds qualitatively to subtidal type motions as were considered by both Durrieu de Madron (1994) and Hickey (1997).

Both Hunkins (1988) and Hickey (1997) observe an-

ticlockwise mean motion along depth contours below the canyon rim. Such motions are consistent with the rectification effects found in the present studies; that is, a mean flow is generated that follows along the canyon flanks from left to right and exits the canyon on the right, facing toward the deep water (see, e.g., Fig. 8a). We recall that the flow direction of the rectified current is independent of the values of the Rossby and temporal Rossby numbers. Thus, the mean current could result from tidal or subtidal oscillations or from other effects. Recent studies by Zhang et al. (1994, 1997) show that rectified flows can occur with the shallow topography on the right in the Northern Hemisphere [i.e., in the same direction observed by Hunkins (1988) and Hickey (1997)] by (i) alongcoast oscillations such as would occur for an alongcanyon tide and (ii) Reynolds stress gradients owing to boundary turbulence generated along the canyon walls with the turbulence decreasing toward the canyon axis, respectively. It is noted that Durrieu de Madron (1994) observed a secondary anticyclonic eddy at the head of Grand Rhone Canyon. This is in the opposite sense than one might expect based on rectified flow arguments. One possible explanation is that the tidal currents in this region were observed to be exceedingly weak.

Hunkins (1988) also observed an upcanyon transport of fluid at the canyon mouth. He speculated that this may be related to tidal rectification. Figure 8a suggests that upcanyon flows are occurring at the lower levels in at least that experiment for which $\mathrm{Ro}_t = 0.5$ and $\mathrm{Ro} = 0.10$. While such measurements were not made at superinertial frequencies such as occur for the semidiurnal tide at Baltimore Canyon, the present experiments suggest that upcanyon flow at deeper levels near the canyon mouth might be expected for a wide range of oscillatory forcing frequencies from subtidal to tidal.

While the Klinck (1996) numerical model studies were for stratified flows, some qualitative similarities are noted between his results and those found herein. As noted previously, he considered the background flow either being from right to left or left to right, not oscillatory as in the present study. Nevertheless, for small Ro_t, the oscillation frequency was small compared to the Coriolis parameter and thus some qualitative similarities might be expected. The first is that for left to right flow, the velocity field was relatively smooth above and below the canyon rim, roughly following canyon isobaths; see his Figs. 2a,b for his weakly stratified case. This is similar to the cyclone regime observations as discussed in the present experiments. The right to left motion in his model, on the other hand, showed a strong cyclonic vorticity, although not a closed cyclone, on the upstream side of the canyon above the rim, similar to that observed in the cyclone regime of Figs. 3, 4, and 5; see his Fig. 4a. Furthermore, this same Fig. 4a indicates that the cyclonic motion on the upstream side of the canyon forces a ''jet'' on the shelf downstream of the canyon, as observed in the present experiments. However, from the limited area presented in Klinck's paper, it does not appear that the jet advects anticyclonically across the continental slope forming a cyclonic vortex as observed in the laboratory.

The flow in his model below the canyon rim (his Fig. 4b) exhibits an upcanyon motion. If one considers the mean of an oscillatory version of the Klinck (1996) model to be an average of his left to right (his Fig. 2b) and right to left (his Figure 4b) results, it is noted that the flow along the canyon axis below the rim is upcanyon, in qualitative agreement with the Hunkins (1988) near-bottom findings and the results found in the present model results.

7. Discussion and concluding remarks

Physical and numerical model experiments have been conducted on an along-isobath oscillatory background flow along a long continental shelf topography interrupted by a single isolated canyon (i.e., a depression). For a fixed geometry and for sufficiently small Ekman (i.e., small viscosity) and Froude numbers, the resulting motion fields are determined by two principal governing parameters, the temporal Rossby and the Rossby numbers. The normalized excursion amplitude of the oscillatory flow $X = \mathrm{Ro}/\mathrm{Ro}_t$ is also shown to be a useful parameter but, as indicated, is not independent of Ro_t and Ro.

For the ranges of Ro_t and Ro considered, two distinct flow regimes were identified in the physical model experiments and verified by the numerical model. At sufficiently large Ro_t and for all Ro investigated, the flow type was designated as cyclone-free in the sense that the background flow on interacting with the bathymetry of the canyon does not separate from the canyon boundaries; that is, no separated flow in the form of large-scale eddy systems is in evidence (see Fig. 2).

For sufficiently small Ro_t and again for the range of Ro investigated, one observes a rather complex flow type designated as the cyclone flow regime; see Figs. 2, 3, 4, and 5. In this regime cyclones are formed both on the right side of the interior of the canyon and to the left of the canyon, facing toward the deep water, as the background flow advects from right to left. The cyclone inside the canyon owes its existence to a combination of shear layer instability as the background flow passes the canyon edge and to vortex stretching as the flow passes over the plunging depth contours. The cyclone on the left owes to the former cyclone forcing an anticyclonic jet to pass over the shelf from right to left, which then plunges over the continental slope, again establishing a cyclone by the process of vortex stretching. The cyclone on the left forms during the phase in the background motion in which the flow is from right to left. If one imagines a mirror image (an anticyclone) of this cyclone on the landward side of the coast, that image would tend to advect the cyclone to the right. These effects tend to cancel, thus allowing the cyclone

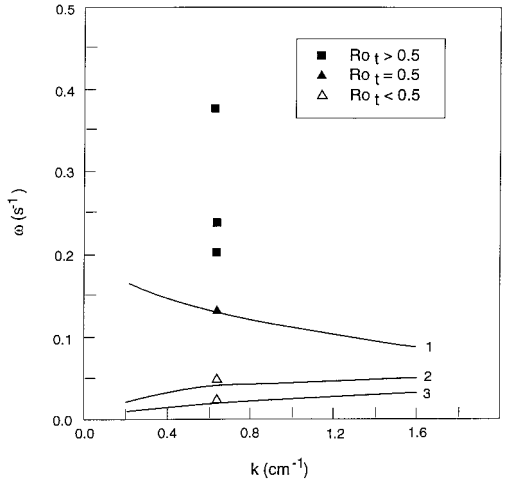

FIG. 18. Plot of the wave frequency against along-shelf wavenumber for the first three modes of topographic Rossby waves for the LEGI physical model obtained from Brink and Chapman (1987); see text.

to remain roughly stationary for a time, allowing the vortex feature to grow.

During the left to right cycle of the background flow, a strong anticyclone is not formed on the left interior side of the canyon because, while the tendency for the shear layer instability is to drive such an anticyclone, the flow passing across plunging depth contours generates cyclonic relative vorticity that, at least partially, opposes the shear layer instability tendency. Furthermore, there is a tendency during the left to right motion to form a cyclonic jet over the shelf (due to the canyon flow following the depth contours), which would then plunge over the shelf to the right of the canyon. This jet would then tend to form a cyclone on the right of the canyon. The mirror image of such a cyclone (and the contribution of the mean flow) would tend to advect the feature to the right, the same direction as the background flow, and thus, unlike in the right to left half cycle, this cyclone would not have time to grow. The cyclone regime is thus a highly asymmetric one in that large-scale eddies are formed during the right to left motion phase, but not in the left to right one.

Asymmetry in the topographic drag in the present experiments, in the sense that the right to left flow leads to the extraction of more kinetic energy from the background flow to the large-scale eddy field than the more smooth left to right flow, leads to strong rectified flows from left to right ''downstream'' of the canyon for the cyclone regime; see also Haidvogel and Brink (1986).

Although the presence of eddies and residual currents point to a high degree of nonlinearity, basic linear ideas have been applied to try to explain the behavior described in Fig. 9, in which the rectified current peaks at $\mathrm{Ro}_t = 0.5$ for all Rossby numbers. Namely, the possibility of a topographic Rossby wave resonant forcing has been investigated. Figure 18 shows the dispersion relations for the first three modes of these waves, computed with the Brink and Chapman (1987) programs for the actual topographic profile of the LEGI shelf and slope. In the present experiments the slope, which supports those waves, is cut by a canyon that forces an alongslope length scale of roughly 1 m. One can see from Fig. 18 that mode 1 is resonantly excited for the corresponding alongshelf wavenumber k ($2\pi/100$ cm) near $\omega = 0.125\ \mathrm{s}^{-1}$ ($\mathrm{Ro}_t = 0.5$). The high eddy activity and attendant mean flow generation observed at $\mathrm{Ro}_t = 0.5$ can then be interpreted as the nonlinear response of the fluid, when the forcing meets this resonance condition. Of course this argument does not provide any details of the nonlinear flow but explains why the system is more nonlinear at $\mathrm{Ro}_t = 0.5$.

This study also included the conduct of a series of numerical experiments for the same range of parameters as considered in the physical experimental studies. For the most part there was good agreement between the numerical studies and the physical experiments. In order to do a parametric study of the physical system considered and at the same time make some direct comparison between the physical and numerical model experiments, measurements of the maximum mean flow generated at a location one canyon width downstream of the canyon axis were made. The normalized data for these mean flow maxima were plotted against the normalized excursion amplitude X; see Fig. 17.

The physical and numerical model results are in good accord in the sense that the maximum mean flow data separate into three distinct regions on this plot. For $X \leq 0.4$, the normalized maximum mean flow is independent of X and is roughly the same order as the mean background speed $\sim 0.6u_0$ (these experiments were in the cyclone regime). For $X \geq 0.4$ the plot separates into (i) a lower branch for which the mean flow is relatively small and increases with X (cyclone-free regime) and (ii) an upper branch for which the mean flow decreases with X (cyclone regime). The branching of the data for small X in Fig. 17 implies that this physical system is not governed by a single parameter X but depends on two parameters (i.e., two of Ro, Ro_t, and X).

Limited numbers of physical model experiments were also conducted to demonstrate the decrease in the maximum value of the mean flow as a function of the downstream coordinate along the shelf break. One experiment was also analyzed that demonstrated that the mean flow in a control volume circumscribing the canyon was divergent at a level near the free surface; that is, there is a net flow out of the control volume with the principal volume flux exiting the canyon region to the right, facing toward the deep water. It was deduced that the most likely source of this volume flux was entering the canyon at large depths from the deep water region. Unfortunately no direct measurements were made of this phenomenon. Owing to the complexity of setting up experiments in the LEGI facility, such measurements cannot be made available for this communication; this,

however, would be a fruitful area for inquiry in the future.

Owing to the very basic nature of the model considered and the limited field observations available for canyon regions, only qualitative comparisons between the two could be made. We are encouraged in the sense that the laboratory experiments exhibit some of the broad characteristics of the field observations. While the physical system considered is a quite simple one, it demonstrates the profound influence topographic variations along a continental shelf can have on the motion fields in the vicinity of the topographic feature (in the present case a canyon). Additionally, it is rather remarkable that the mean flows generated can be of the same order as the characteristic magnitude of the background current forcing the motion. The work opens the way for more complex studies that could investigate such matters as (i) cross-shelf transports in the vicinity of a canyonlike feature, (ii) the effects of ridges and isolated seamounts on the shelf, (iii) the influence of background stratification, (iv) the importance of turbulence, and (v) applications to specific geographical locations.

Acknowledgments. Support of the Physical Oceanography Program of the National Science Foundation under Grant OCE-9301572 is gratefully acknowledged. This work was also partially supported by CNRS-SDU and by Grant EPSHOM/CMO 7/95. The authors wish to extend their thanks to Mr. Rene Carcel and Mr. Henri Didelle for their effective technical support to the LEGI physical modeling portions of the study. The authors are grateful to Dr. Bernard Le Cann for his discussions related to resonant forcing of Rossby waves. Finally, the authors wish to thank the anonymous referees for their helpful suggestions made to improve the manuscript.

REFERENCES

Allen, J. S., 1976: Continental shelf waves and alongshore variations in bottom topography and coastline. *J. Phys. Oceanogr.,* **6,** 864–878.

Allen, S. E., 1996: Topographically generated, subinertial flows within a finite length canyon. *J. Phys. Oceanogr.,* **26,** 1608–1632.

Baines, P. G., 1983: Tidal motion in submarine canyons: A laboratory experiment. *J. Phys. Oceanogr.,* **13,** 310–328.

Batchelor, G. K., 1970: *An Introduction to Fluid Dynamics.* Cambridge University Press, 615 pp.

Bleck, R., C. Rooth, D. Hu, and L. Smith, 1992: Salinity-driven thermocline transients in a wind- and thermohaline-forced isopycnic coordinate model of the North Atlantic. *J. Phys. Oceanogr.* **22,** 1486–1505.

Blumberg, A. F., and G. L. Mellor, 1987: A description of a three-dimensional coastal ocean circulation model. *Three-Dimensional Coastal Ocean Models,* C. Mooers, Ed., *Coastal and Estuarine Sciences,* Vol. 4, Amer. Geophys. Union, 1–16.

Boyer, D. L., and X. Zhang, 1990: The interaction of time-dependent rotating and stratified flow with isolated topography. *Dyn. Atmos. Oceans,* **14,** 543–575.

——, G. Chabert d'Hieres, H. Didelle, J. Verron, R. Chen, and L. Tao, 1991: Laboratory simulation of tidal rectification over seamounts: Homogeneous model. *J. Phys. Oceanogr.,* **21,** 1559–1579.

Brink, K. H., 1986: Topographic drag due to barotropic flow over the continental shelf and slope. *J. Phys. Oceanogr.,* **16,** 2150–2158.

——, and D. C. Chapman, 1987: Programs for computing properties of coastal-trapped waves and wind-driven motions over the continental shelf and slope. 2d ed. WHOI Tech. Rep. [Available from Co-op Program, Woods Hole Oceanographic Institution, 93 Water St., Woods Hole, MA 02543-1050.]

Bryan, K., 1969: A numerical method for the study of the circulation of the world ocean. *J. Comput. Phys.,* **4,** 347–376.

Brylinski, J. M., and Y. L. Lagadeuc, 1990: The inshore/offshore waters interface off the French coast in Dover Strait: A frontal area. *Cah. Roy. Acad. Sci. Paris,* **t. 311,** Series II, 535–540.

Butman, B., R. C. Beardsley, B. Magnell, D. Frye, J. A. Vermesch, R. Schiltz, R. Limeburner, W. R. Wright and M. A. Noble, 1982: Recent observations of the mean circulation on Georges Bank. *J. Phys. Oceanogr.,* **12,** 569–591.

Cannon, G. A., and G. S. E. Lagerloef, 1983: Topographic influence on coastal circulation: A review. *Coastal Oceanography,* H. Glade, A. Edwards, and H. Svendson, Eds., Plenum Publishing, 235–252.

Church, T. M., C. N. K. Mooers, and A. D. Voorhis, 1984: Exchange processes over a middle Atlantic bight shelfbreak canyon. *Estuar. Coastal Shelf Sci.,* **19,** 393–411.

Cox, M. D., 1984: A primitive equation three-dimensional model of the ocean. GFDL Ocean Group Tech. Rep. 1, Princeton University, 250 pp. [Available from Geophysical Fluid Dynamics Laboratory, Forrestal Campus, U.S. Route 1, P.O. Box 308, Princeton, NJ 08542.]

Durrieu de Madron, X., 1994: Hydrography and nepheloid structure in the Grand-Rhone canyon. *Contin. Shelf. Res.,* **14,** 457–477.

Eriksen, C., 1991: Observations of amplified flow atop a large seamount. *J. Geophys. Res.,* **96,** 15 th227–15 236.

Freeland, H. J., and K. L. Denman, 1982: A topographically controlled upwelling center off southern Vancouver Island. *J. Mar. Res.,* **40**(4), 1069–1093.

——, and P. McIntosh, 1989: The vorticity balance on the southern British Columbia continental shelf. *Atmos.–Ocean,* **27,** 643–657.

Garreau, P., and R. Mazé, 1992: Tidal rectification and mass transport over a shelf break: A barotropic frictionless model. *J. Phys. Oceanogr.,* **22,** 719–731.

Genin, A., M. Noble, and P. F. Lonsdale, 1989: Tidal currents and anticyclonic motions on two North Pacific seamounts. *Deep-Sea Res.,* **36,** 1803–1816.

Greenspan, H. P., and L. N. Howard, 1963: On a time-dependent motion of a rotating fluid. *J. Fluid Mech.,* **22,** 449–462.

Grimshaw, R. H. J., P. G. Baines, and R. C. Bell, 1985: The reflection and diffraction of internal waves from the junction of a slit and a half-space, with applications to submarine canyons. *Dyn. Atmos. Oceans,* **9,** 85–120.

Haidvogel, D. B., and K. H. Brink, 1986: Mean currents driven by topographic drag over the continental shelf and slope. *J. Phys. Oceanogr.,* **16,** 2159–2171.

——, and A. Beckman, 1995: Wind-driven residual currents over a coastal canyon. *Proc. Hawaiian Winter Workshop on Topographic Effects in the Ocean,* P. Muller and D. Henderson, Eds., School of Ocean and Earth Science and Technology, University of Hawaii, 219–224.

——, J. Wilken, and R. Young, 1991: A semi-spectral primitive equation ocean circulation model using vertical sigma and orthogonal curvilinear horizontal coordinates. *J. Comput. Phys.,* **94,** 151–185.

Hedstrom, K. S., 1994: User's manual for a semi-spectral primitive equation ocean circulation model. Version 3.9. Institute of Marine and Coastal Sciences, Rutgers University, 131 pp. [Available from Institute of Marine and Coastal Sciences, Rutgers University, P.O. Box 231, New Brunswick, NJ 08903.]

Hickey, B. M., 1989: Patterns and processes of circulation over the

Washington continental shelf and slope. *Coastal Oceanography of Washington and Oregon,* M. Landry and B. Hickey, Eds., Elsevier Science, 41–116.

——, 1995: Coastal submarine canyons. *Proc. Hawaiian Winter Workshop on Topographic Effects in the Ocean,* P. Muller and D. Henderson, Eds., School of Ocean and Earth Science and Technology, 95–110.

——, 1997: The response of a steep-sided, narrow canyon to time-variable wind forcing. *J. Phys. Oceanogr.,* **27,** 697–726.

——, E. Baker, and N. B. Kachel, 1986: Suspended particle movement in and around Quinault Submarine Canyon. *Mar. Geol.,* **71,** 35–83.

Hotchkiss, F. S., and C. Wunsch, 1982: Internal waves in Hudson Canyon with possible geological implications. *Deep-Sea Res.,* **29,** 415–422.

Hunkins, K., 1988: Mean and tidal currents in Baltimore Canyon. *J. Geophys. Res.,* **93,** 6917–6929.

Huthnance, J. M., 1973: Tidal current asymmetries over the Norfolk Sandbanks. *Estuar. Coastal Mar. Sci.,* **1,** 89–99.

——, 1981: On the mass transports generated by tides and long waves. *J. Fluid Mech.,* **102,** 367–387.

——, 1995: Circulation, exchange and water masses at the ocean margin: The role of physical processes at the shelf edge. *Progress in Oceanography,* Vol. 35, Pergamon, 353–431.

Inman, D. L., C. E. Nordstrom, and R. E. Flick, 1976: Currents in submarine canyons: An air-sea-land interaction. *Annu. Rev. Fluid Mech.,* **8,** 275–310.

Iskandarani, M., D. B. Haidvogel, and J. P. Boyd, 1995: A staggered spectral element model with applications to the oceanic shallow water equations. *Int. J. Num. Methods Fluids,* **20,** 393–414.

Kinsella, E. D., A. E. Hay, and W. W. Denner, 1987: Wind and topographic effects on the Labrador Current at Carson Canyon. *J. Geophys. Res.,* **92**(C10), 10 853–10 869.

Klinck, J. M., 1988: The influence of a narrow transverse canyon on initially geostrophic flow. *J. Geophys. Res.,* **93,** 509–515.

——, 1989: Geostrophic adjustment over submarine canyons. *J. Geophys. Res.,* **94,** 6133–6144.

——, 1996: Circulation near submarine canyons: A modeling study. *J. Geophys. Res.,* **101,** 1211–1223.

Loder, J. W., 1980: Topographic rectification of tidal currents on the sides of Georges Bank. *J. Phys. Oceanogr.,* **10,** 1399–1416.

——, and D. G. Wright, 1985: Tidal rectification and frontal circulation on the sides of Georges Bank. *J. Mar. Res.,* **43,** 581–604.

Lueck, R. G., and T. R. Osborn, 1985: Turbulence measurements in a submarine canyon. *Contin. Shelf Res.,* **4**(6), 681–695.

Nguyen, T., and J. Verron, 1995: Effets d'une topographie sous-marine à moyenne echelle sur un ecoulement uniforme dans un canal: Etude à l'aide d'un modele aux equations primitives à frontieres ouvertes. *Oceanol. Acta,* **19,** 27–40.

Noble, M., and B. Butman, 1989: The structure of subtidal currents within and around Lydonia Canyon: Evidence for enhanced cross-shelf fluctuations over the mouth of the canyon. *J. Geophys. Res.,* **94,** 8091–8110.

Pedlosky, J., 1979: *Geophysical Fluid Dynamics.* Springer-Verlag, 624 pp.

Pingree, R. D., and B. Le Cann, 1990: Structure, strength and seasonality of the slope currents in the vicinity of the Bay of Biscay region. *J. Mar. Biol. Assoc. UK,* **70,** 857–885.

Prandtl, L., and O. G. Tietgens, 1934: *Fundamentals of Hydro- and Aeromechanics.* Dover, 270 pp.

Shepard, F. P., R. Reville, and R. S. Dietz, 1939: Ocean-bottom currents off the California coast. *Science,* **89,** 488–489.

——, N. F. Marshall, P. A. McLoughlin, and G. G. Sullivan, 1979: *Currents in Submarine Canyons and Other Seavalleys.* Amer. Assoc. Petrol. Geol., Studies in Geology No. 8, 173 pp. [Available from Amer. Assoc. Petrol. Geol., Box 979, Tulsa, OK 74101.]

Stetson, H. C., 1936: Geology and paleontology of the Georges Bank canyons, part 1, geology. *Geol. Soc. Amer. Bull.,* **47,** 339–366.

Stommel, H., 1954: Serial observations of drift currents in the Central North Atlantic Ocean. *Tellus,* **6,** 204–214.

Tee, K. T., 1979: The structure of three-dimensional tide generating currents, I. Oscillatory currents. *J. Phys. Oceanogr.,* **9,** 930–944.

——, 1980: The structure of three-dimensional tide generating currents, II. Residual currents. *J. Phys. Oceanogr.,* **10,** 2035–2057.

——, 1985: Depth-dependent studies of tidally induced residual currents on the sides of Georges Bank. *J. Phys. Oceanogr.,* **15,** 1818–1846.

Verron, J., D. Renouard, D. L. Boyer, G. Chabert d'Hieres, T. Nguyen, and H. Didelle, 1995: Rectified flows over an elongated topographic feature along a vertical wall. *J. Phys. Oceanogr.,* **25,** 2185–2203.

Wang, D. P., 1980: Diffraction of continental shelf waves by irregular longshore geometry. *J. Phys. Oceanogr.,* **10,** 1187–1199.

Wilken, J. L., and D. C. Chapman, 1990: Scattering of coastal trapped waves by irregularities in coastline and topography. *J. Phys. Oceanogr.,* **20,** 396–421.

Zhang, X., and D. L. Boyer, 1993: Laboratory study of rotating, stratified, oscillatory flow over a seamount. *J. Phys. Oceanogr.,* **23,** 1122–1141.

——, ——, G. Chabert d'Hieres, and D. Aelbrecht, 1994: Rectified flow of a rotating fluid along a vertical sidewall. *Phys. Fluids,* **6**(4), 1440–1453.

——, ——, N. Perenne, and D. Renouard, 1996: Mean flow generation along a sloping region in a rotating homogeneous fluid. *J. Geophys. Res.,* **101,** 28 597–28 614.

——, ——, and H. J. S. Fernando, 1997: Turbulence-induced rectified flow in rotating fluids. *J. Fluid Mech.,* in press.

Zimmerman, J. T. F., 1978: Topographic generation of residual circulation by oscillatory (tidal) currents. *Geophys. Astrophys. Fluid Dyn.,* **11,** 35–47.

——, 1980: Vorticity transfer by tidal currents over an irregular topography. *J. Mar. Res.,* **38,** 601–630.